THE PLANT CELL

The Plant Cell, 2025, **37**, koaf201

https://doi.org/10.1093/plcell/koaf201
Advance access publication 14 August 2025
Research Article

The receptor-like cytoplasmic kinase AeRLCK2 mediates Nod-independent rhizobial symbiosis in *Aeschynomene* legumes

Natasha Horta Araújo,[1,*†] David Landry,[2,†,‡] Johan Quilbé,[1,†,‡] Marjorie Pervent,[1] Nico Nouwen,[1] Christophe Klopp,[3,4] Julie Cullimore,[2] Djamel Gully,[1] Céline Vicedo,[2] Virginie Gasciolli,[2] Laurent Brottier,[1] Carole Pichereaux,[5,6,7] Martin Racoupeau,[3,4] Maëlle Rios,[1] Frédéric Gressent,[1] Clémence Chaintreuil,[1] Clare Gough,[2] Eric Giraud,[1] Benoit Lefebvre,[2,*] Jean-François Arrighi[1,*]

[1]PHIM Plant Health Institute, Université de Montpellier, IRD, INRAE, CIRAD, Institut Agro, Campus de Baillarguet, Montpellier 34398, France
[2]Laboratory of Plant-Microbe-Environment Interactions (LIPME), Université de Toulouse, INRAE, CNRS, Castanet-Tolosan 31326, France
[3]Université de Toulouse, INRAE, BioinfOmics, GenoToul Bioinformatics Facility, Castanet-Tolosan 31326, France
[4]Université de Toulouse, INRAE, UR 875 MIAT, Castanet-Tolosan 31326, France
[5]Fédération de Recherche Agrobiosciences, Interactions et Biodiversité (FRAIB), Université de Toulouse, CNRS, Université Toulouse III—Paul Sabatier (UT3), Auzeville Tolosan 31320, France
[6]Institut de Pharmacologie et de Biologie Structurale (IPBS), Université de Toulouse, CNRS, Université Toulouse III—Paul Sabatier (UT3), Toulouse 31400, France
[7]Infrastructure nationale de protéomique, ProFI, Toulouse FR 2048, France
*Author for correspondence: jean-francois.arrighi@ird.fr (J.-F.A.), hortanatasha@hotmail.com (N.H.A.), benoit.lefebvre@inrae.fr (B.L.)
†These authors contributed equally to this work.
‡Present address: Department of Molecular Biology and Genetics, Aarhus University, Denmark.
The authors responsible for distribution of materials integral to the findings presented in this article in accordance with the policy described in the Instructions for Authors (https://academic.oup.com/plcell/pages/General-Instructions) are Jean-François Arrighi (jean-francois.arrighi@ird.fr) and Benoit Lefebvre (benoit.lefebvre@inrae.fr).

Abstract

Many plants interact symbiotically with arbuscular mycorrhizal fungi to enhance inorganic phosphorus uptake, and legumes also develop a nodule symbiosis with rhizobia for nitrogen acquisition. The establishment and functioning of both symbioses rely on a common plant signaling pathway activated by structurally related Myc and Nod factors. Recently, a SPARK receptor-like kinase (RLK)/receptor-like cytoplasmic kinase (RLCK) complex was shown to be essential for arbuscular mycorrhiza formation in both monocot and dicot plants. Here, we show that in *Aeschynomene* legumes, the RLCK component of this receptor complex has undergone a gene duplication event and mediates a unique nodule symbiosis that is independent of rhizobial Nod factors. In *Aeschynomene evenia*, *AeRLCK2* is crucial for nodule initiation but not for arbuscular mycorrhiza symbiosis. Additionally, AeRLCK2 physically interacts with and is phosphorylated by the cysteine-rich RLK, AeCRK, which is also required for nodulation. This finding uncovers an important molecular mechanism that controls the establishment of nodulation and is associated with Nod-independent symbiosis.

Introduction

Plants have evolved a range of mutualistic partnerships with soil-dwelling microorganisms to enhance their nutrient uptake. The oldest and most widespread symbiosis is the association with Glomeromycotina fungi, referred to as arbuscular mycorrhizal (AM) fungi. AM fungi develop extensive hyphal networks to take up inorganic phosphorus (Pi) and other nutrients from the soil. They also colonize plant roots and form intracellular branched structures called arbuscules, through which they provide these nutrients to plants (Rich et al. 2021). Plant species within the nitrogen (N)-fixing clade are able to develop an additional symbiosis with diazotrophic bacteria that are hosted in root nodules (van Velzen et al. 2019). This interaction allows the plants to access the abundant atmospheric N by converting it into ammonium (Roy et al. 2020). By providing Pi and N to the plants, these symbioses are central to the functioning of natural ecosystems and the productivity of agro-systems.

Genetic studies of *Oryza sativa* (rice) and model legumes (such as *Lotus japonicus* and *Medicago truncatula*), establishing a symbiosis with AM fungi and/or rhizobia, have demonstrated that the evolution of nitrogen-fixing symbiosis has co-opted perception, signaling, and infection mechanisms essential for the establishment of AM (Radhakrishnan et al. 2020). Chitooligosaccharides (COs) and lipochitosaccharides (LCOs) produced by AM fungi and LCOs produced by rhizobia (known as Nod factors) are perceived by distinct plasma membrane receptor-like kinases of the LysM-RLK subfamily (Buendia et al. 2018; Feng et al. 2019; Ding et al. 2024, 2025; Zhang et al. 2024). These signals are then transduced by SymRK (Symbiosis Receptor Kinase), a RLK belonging to the LRR-RLK subfamily, which initiates a common symbiosis signaling pathway leading to transcriptional reprograming (Gobbato 2015; Roy et al. 2020).

Received March 31, 2025. Accepted June 17, 2025.

This transcriptional reprogramming drives infection by both AM fungi and rhizobia, culminating in their intracellular accomodation either into the plant root or into nodules (Roy et al. 2020). Another RLK belonging to the SPARK-RLK subfamily, KIN3 (KINASE 3), is crucial for the arbuscule formation during AM (Irving et al. 2022; Leng et al. 2023). Recently, KIN3 has been shown to interact with 2 receptor-like cytoplasmic kinase (RLCK) paralogs, ARBUSCULAR MYCORRHIZA-INDUCED KINASES 8 and 24 (AMK8 and AMK24), which also play a key role in arbuscule formation in *L. japonicus* (Leng et al. 2023). This RLK/RLCK complex was found to have a conserved role in AM in rice (Bravo et al. 2016; Roth et al. 2018; Montero et al. 2021; Leng et al. 2023). Interestingly, *KIN3* orthologs are only found in plants able to form AM and *KIN3* is dispensable for rhizobial symbiosis in *M. truncatula* (Irving et al. 2022). This questions whether the KIN3-interacting RLCKs are required or not for nodulation.

We challenged this view through the genetic analysis of nodulation in *Aeschynomene evenia*. This legume species has emerged as a model of choice for the study of a unique N-fixing symbiosis with photosynthetic *Bradyrhizobium* strains that do not produce Nod factors (Arrighi et al. 2012; Chaintreuil et al. 2016). In this process, bacteria intensely colonize crowns of axillary root hairs (ARHs) located at lateral root bases that are the initial sites for bacterial entry. From there, they progress intercellularly towards the root cortex, where a nodule primordium finally forms (Horta Araújo et al. 2024). While the nature of the bradyrhizobial signals that activate this so-called Nod-independent symbiosis remain to be identified, progress has been made on the plant side in recent years, thanks to the availability of a reference genome and a collection of ethyl methane sulfonate (EMS) nodulation mutants for *A. evenia* (Quilbé et al. 2021, 2022). It is now known that many components of the common symbiotic signaling pathway are conserved in *A. evenia* but that this pathway is likely activated by other type of receptor proteins. Notably, a Cysteine-rich RLK, AeCRK, was recently shown to be required to establish the Nod-independent symbiosis (Quilbé et al. 2021, 2022).

In this work, we identified *AeRLCK2*, a *RLCK* homolog to *L. japonicus AMK8*, as required for the Nod-independent symbiosis. Through the genetic, phenotypic and molecular characterization of allelic mutants, we show that *AeRLCK2* is essential for nodulation but dispensable for AM. Furthermore, we provide evidence that *AeRLCK2* originated from a recent tandem duplication event and offer clues to explain how it has evolved for a role in the Nod-independent symbiosis. Finally, we demonstrate that AeRLCK2 physically interacts with and serves as a phosphorylation substrate for AeCRK. These findings shed light on the evolution of RLCKs in plant symbioses and further elucidate the mechanisms by which the Nod-independent nodulation process is triggered in *Aeschynomene* legumes.

Results

Mutant-based identification of AeRLCK2, a symbiosis receptor-like cytoplasmic kinase

To identify genes involved in establishment of the Nod-independent symbiosis, we analyzed a set of 12 uncharacterized nodulation mutants obtained from screening in greenhouse conditions of an EMS-mutagenized population of *A. evenia* CIAT22838 (Supplementary Table S1) (Quilbé et al. 2021). The common characteristic of these mutants is that most plants in each mutant line had a Nod- phenotype similar to *ccamk-2* mutant plants (Quilbé et al. 2022), while a few plants formed 1 or few enlarged nodules, when inoculated with the photosynthetic *Bradyrhizobium* strain sp. ORS278, (Fig. 1A). This type of nodulation was qualified as a Big Nodule (BN) phenotype. For these mutants, Nod- plants displayed typical nitrogen starvation symptoms (reduced plant growth and yellow leaves), whereas BN plants were better developed with green leaves, indicating that the formed BN nodules had nitrogen-fixing activity (Fig. 1B).

Phenotypic analysis of F2 progeny generated from crosses between the WT line and the 12 nodulation mutants revealed that they segregated in a 3:1 ratio of plants with a WT-like nodulation phenotype (with numerous and normal sized pink nodules) to plants with either a Nod- or BN phenotype, respectively (Supplementary Table S2). These data confirmed the dual mutant phenotype and demonstrated the monogenic and recessive nature of each mutation. To identify the gene(s) responsible for this dual nodulation phenotype, we performed a mapping-by-sequencing approach on bulked F2 mutant plants for 8 mutants. Linkage mapping repeatedly identified the same locus near the end of the Ae01 chromosome, with all mutations located in the Ae01g26600 gene (Fig. 1C, Supplementary Fig. S1 and Supplementary Table S2). Given these results, we amplified and sequenced the Ae01g26600 gene in the remaining 4 mutants and all had mutations (Supplementary Table S2). Further allelism tests between the 12 mutants showed that they belonged to the same complementation group, clearly establishing the Ae01g26600 mutations as responsible for the dual Nod-/BN phenotype (Supplementary Table S3).

Blast analysis revealed that Ae01g26600 codes for a RLCK (receptor-like cytoplasmic kinase), a subtype of RLK that lacks lack extracellular ligand-binding domains (Lin et al. 2013; Liang and Zhou 2018). However, we observed that the coding sequence (CDS) of Ae01g26600 was twice as long as that of other *RLCK* genes. Consistent with this, *A. evenia* RNAseq datasets showed that there are actually 2 different *RLCK* genes at the Ae01g26600 locus (Chaintreuil et al. 2016; Quilbé et al. 2021). This suggested that the Ae01g26600 gene is misannotated in the current *A. evenia* reference genome. We corrected this by manually delineating the 2 genes organized in tandem and named them *AeRLCK1* and *AeRLCK2*. As all 12 identified mutations were in the *AeRLCK2* gene, we numbered the corresponding allelic mutants *rlck2-1* to *rlck2-12* (Fig. 1D and Supplementary Table S2).

To validate our curated annotation, the *AeRLCK2* CDS was amplified from WT *A. evenia* cDNAs and cloned downstream a *L. japonicus* ubiquitin promoter (*pLjUb*). Using *Agrobacterium rhizogenes*-mediated hairy root transformation, the construct was introduced into the roots of the strong allele mutant *rlck2-11*, characterized by a nonsense mutation. WT-like nodulation was restored in *rlck2-11* (Fig. 1E and Supplementary Table S4). Functional annotation of the 403 amino acid AeRLCK2 predicted the presence of a transmembrane domain followed by a serine/threonine kinase domain, where all mutations were identified (Fig. 1D). We speculated that AeRLCK2 encodes a symbiosis plasma membrane-localized RLCK whose kinase domain integrity is essential to mediate signal transduction.

AeRLCK2 perfoms a key function in rhizobial symbiosis

To characterize in more detail the role of *AeRLCK2* in nodulation, we performed in vitro growth chamber nodulation assays with *Bradyrhizobium* ORS278 on 4 mutant lines, *rlck2-1*, *rlck2-5*, *rlck2-10* and *rlck2-11*, using the WT line and *ccamk-2* mutant as controls. Nodulation kinetics revealed that in the WT line, nodules were pink at 10 dpi while in the *rlck2* mutants the first BN nodules

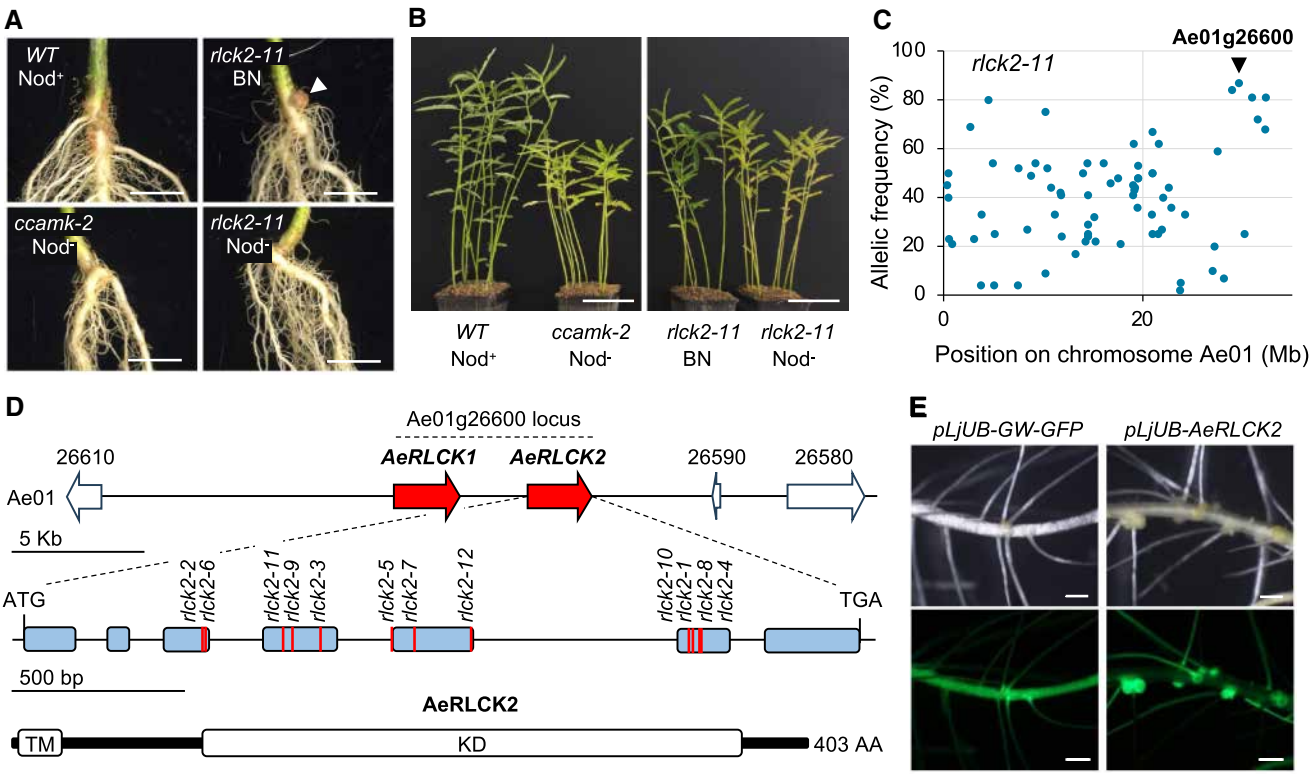

Figure 1. Mutant-based identification of *AeRLCK2* as required for Nod-independent symbiosis. **A)** Root phenotypes of Wilde Type (WT), *ccamk-2* and *rlck2-11* plants at 28 dpi with *Bradyrhizobium* ORS278 strain and grown in greenhouse conditions. Nod^+: presence of WT nodules, Nod^-: Absence of nodules, BN: Big Nodule (white arrowhead). Scale bar: 1 cm. **B)** Aerial phenotypes of the same plants grown for 15 additional days in greenhouse conditions after analysis of their root nodulation. Scale bar: 10 cm. **C)** Frequency of EMS-induced mutant alleles in pools of Nod^- backcrossed F2 plants derived from the *rlck2-11* mutant using mapping-by-sequencing. The SNP corresponding to the putative causal mutation in *rlck2-11* is marked with a black arrowhead. **D)** *AeRLCK2* gene and protein structure. Upper panel: genomic region of chromosome Ae01 containing the Ae01g26600 locus. Filled arrows indicate *RLCK* genes. Middle panel: gene structure of AeRLCK2. Blue boxes represent exons and red lines indicate the positions of the EMS mutations in the *rlck2* mutants. Bottom panel: domain structure of the predicted AeRLCK2 protein. White boxes indicate the positions of the predicted domains: TM for transmembrane domain and KD for kinase domain. **E)** Functional complementation of *A. evenia rlck2-11*. Hairy roots of *rlck2-11* transformed with either the empty vector (left images) or containing the *AeRLCK2* CDS under the control of p*LjUb* (right images) at 14 dpi with *Bradyrhizobium* ORS278. GFP (Green Fluorescent Protein) was used as a plant transformation marker. Scale bar: 500 µm.

emerged at 14 dpi (Supplementary Fig. S2). At 21 dpi, the nodulation frequency of the plants was 100% for WT, with each plant containing numerous nodules, and 0% for the *ccamk-2* mutant plants. In contrast, 30% to 80% of the *rlck2* mutant plants were devoid of nodules, while the others contained 1 or a few BNs (see below) (Fig. 2A). This points to an important role of *AeRLCK2* in nodule formation.

Interestingly, inoculated roots of both Nod- and BN *rlck2* plants displayed well-developped crowns of ARHs at lateral root bases, similar to noninoculated plants and the *ccamk-2* mutant (Nod- strict), whereas on inoculated WT roots these ARHs were small (Fig. 2B). In *A. evenia*, these ARHs are the first colonization sites of bradyrhizobia and their development is tightly controlled by the nitrogen status of the plant (Quilbé et al. 2022). Kinetics of ARH development showed that they develop over time in uninoculated WT plants, whereas their development is suppressed in inoculated WT plants (Fig. 2C). No such *Bradyrhizobium*-induced repression of ARH development was observed in *rlck2* and *ccamk-2* mutants. This observation led us to analyse at which stage infection is blocked in *rlck2* mutants. X-Gluc staining of ORS278-GUS inoculated *rlck2-11* mutant roots at 21 dpi revealed intense blue staining on the surface and between the ARHs, but no penetration into the inner root cortex was observed (except for the BN), similar to the *ccamk-2* mutant (Fig. 2D). In contrast, *crk* mutants, which develop small bumps containing infection pockets after inoculation (Quilbé et al. 2022), showed reduced ARH development in the presence of ORS278 (Supplementary Fig. S3). RT-qPCR analysis of 6 symbiosis-induced marker genes, *NODULE INCEPTION* (*AeNIN*), *VAPYRIN* (*AeVPY*), *Symbiotic REMORIN 1* (*AeSymREM1*), *EARLY NODULIN 40* (*AeENOD40*), *SUBTILASE* (*AeSBT*) and *AeCRK* (Quilbé et al. 2022), showed no induction of their expression in *rlck2-11* and *ccamk-2* inoculated with the ORS278 strain (Fig. 2E). Taken together, these results indicate that the mutations in *AeRLCK2* block early symbiosis responses.

Additionally, *rlck2* mutant plants showed a drastic decrease in nodule numbers. WT plants contained an average of 35 nodules per root at 21 dpi, while roots of most nodulated *rlck2* mutant plants exhibited only 1 or 2 BN nodules (Fig. 3A). These BNs had an average diameter that was twice as large as that of WT nodules (Fig. 3B). We interpret this as a compensatory mechanism for their very few numbers in *rlck2* mutants. Roots of *rlck2* mutant plants containing BN nodules had nitrogenase enzyme activity, as measured by the acetylene reduction assay (ARA), and accordingly these plants carried green leaves (Fig. 3C, Supplementary Fig. S4). Light microscopy analysis of BN nodule sections from *rlck2-11* plants showed that they had a similar structure to WT nodules, with a central tissue infected by bacteria and a peripheral uninfected nodule cortex containing vascular bundles (Fig. 3D). However, very often these BN nodules also contained small necrotic zones and brown spots. These areas had an intense

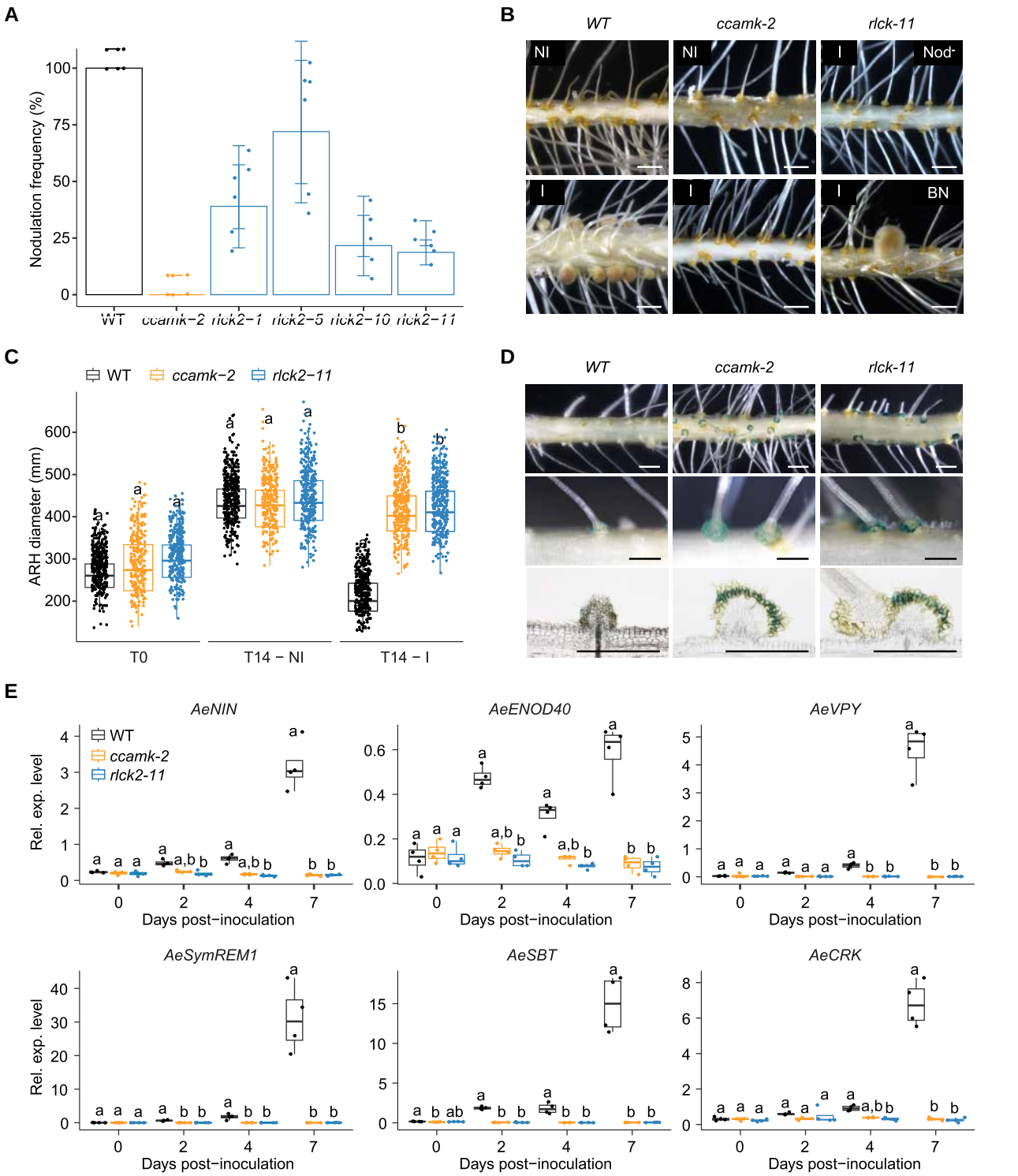

Figure 2. *Bradyrhizobium* infection and symbiotic signaling in *rlck2* mutants. **A)** Frequency of nodule occurrence at 21 dpi in Wild Type (WT), *ccamk*-2, *rlck2*-1, *rlck2*-5, *rlck2*-10 and *rlck2*-11 plants. Error bars represent SD ($n = 3$ biological replicates from independent experiments, with at least 15 plants per line in each replicate). **B)** Comparison of root nodulation phenotypes in WT, *ccamk*-2 and *rlck2*-11, under noninoculated (NI) or *Bradyrhizobium* ORS278-inoculated (I) plants at 21 dpi. Note the presence of either a Nod$^-$ or an BN phenotype in *rlck2*-11 inoculated roots. Scale bar: 1 mm. **C)** ARH diameter in WT, *ccamk*-2 and *rlck2*-11 at different time-points in noninoculated (NI) and inoculated (I) plants with *Bradyrhizobium* ORS278. T0: time 0. T14: time 14 d after inoculation or not. Dots represent individual measurements. **D)** ARH colonization of WT, *ccamk*-2 and *rlck2*-11 plants at 21 dpi with GUS-tagged ORS278, observed on whole roots (upper and middle panels) and root sections (lower panels). Scale bars: 1 mm (upper panels) and 0.5 mm (middle and lower panels). **E)** Expression of nodulation-induced gene in WT, *ccamk*-1 and *rlck2*-11 plants. Relative expression levels (Rel. exp. level) of *AeNIN* (NODULE INCEPTION), *AeSymREM1* (Symbiotic REMORIN 1), *AeENOD40* (EARLY NODULIN 40), *AeSBT* (SUBTILASE), *AeVPY* (VAPYRIN) and *AeCRK* (Cystein-rich Receptor-like Kinase) were measured by RT-qPCR in plant roots at 0, 2, 4 and 7 dpi. The results were normalized against *AeEF1a* and *Ubiquitin* housekeeping genes. Data presented in boxplots correspond to 4 biological replicates, each derived from independent experiments, with at least 5 plants per line in each replicate. Different letters indicate significant differences between conditions as determined by analysis of variance (Kruskal-Wallis) and post-hoc analysis (Dunn's test), $P < 0.05$. Box plots showing the median (bold segment), interquartile range (box from Q1 to Q3), minimum and maximum (whiskers), and outliers (individual points).

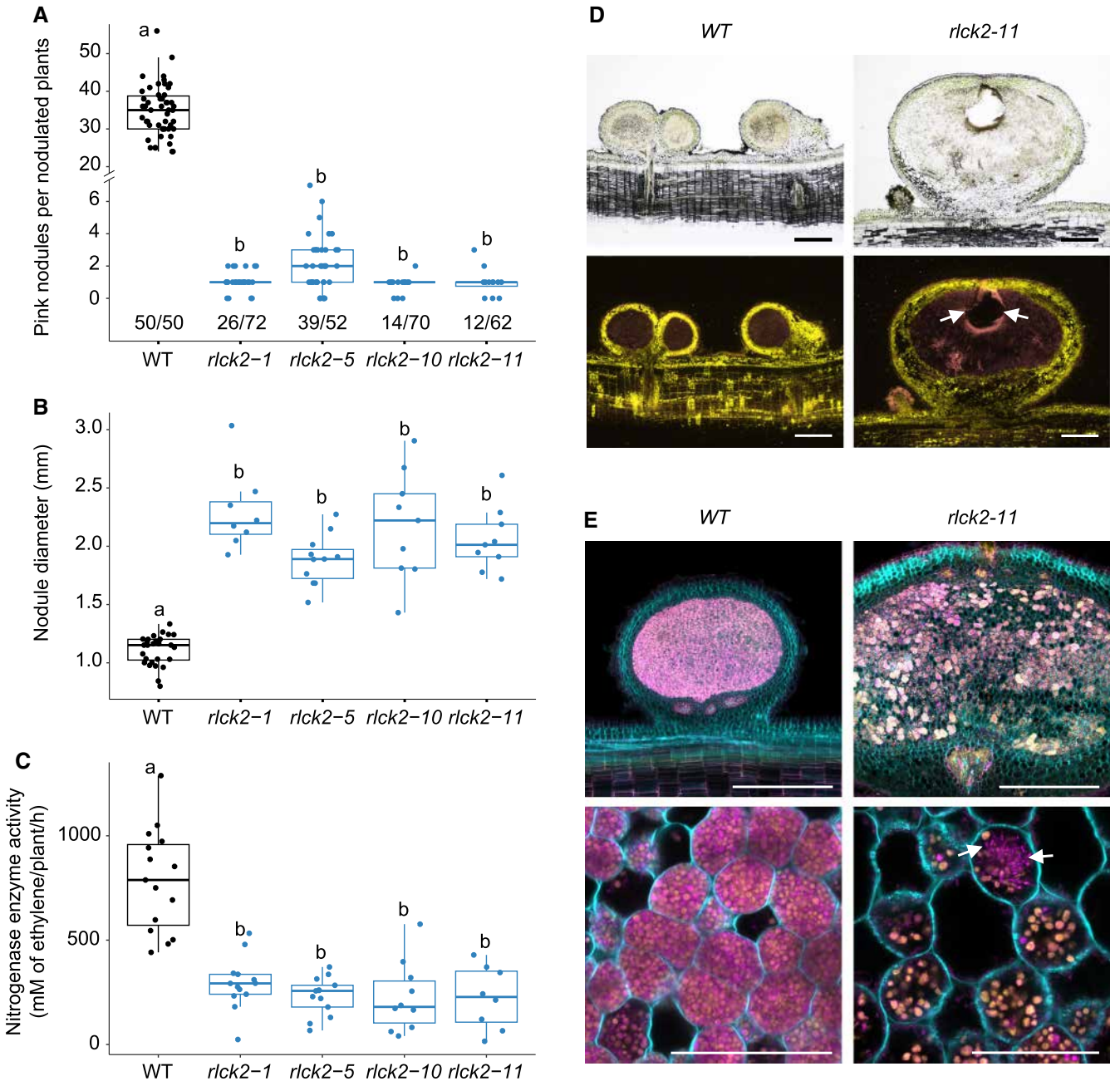

Figure 3. Nodule development and colonization by *Bradyrhizobium* in *rlck2* mutants. **A)** Number of pink nodules formed on nodulated plants in Wild Type (WT), *rlck2-1*, *5*, *10* and *11* plants at 21 dpi with *Bradyrhizobium* ORS278. Numbers below the boxplots indicate the number of nodulated plants relative to the total number of inoculated plants. **B)** Nodule diameter and **C)** nitrogenase enzyme activity measured by ARA ($n \geq 3$ nodulated roots per line and biological replicate) from the same plants as in **A**. Data in **A** to **C** correspond to 3 biological replicates from independent experiments. Dots represent individual plants. Letters indicate significant differences between conditions, as determined by analysis of variance (Kruskal-Wallis) and post-hoc analysis (Dunn's test), $P < 0.05$. Box plots showing the median (bold segment), interquartile range (box from Q1 to Q3), minimum and maximum (whiskers), and outliers (individual points). **D)** Cross-sections of WT and *rlck2-11* nodules observed under brightfield (top) or FITC filter (bottom). Yellow/green fluorescence was pseudocolored in magenta, and red fluorescence was pseudocolored in yellow for visualization purposes. White arrows indicate the occurrence of defense-like responses within the nodule. Scale bar: 500 μm. **E)** Cytological analysis of nodule cross-sections from WT and *rlck2-11* plants using a confocal microscope after staining with SYTO9 (live bacteria), propidium iodide (infected plant nuclei and dead bacteria or bacteria with a compromised membrane) and calcofluor (plant cell wall). For visualization purposes, SYTO 9 (originally green) was pseudocolored in magenta, propidium iodide (originally red) in yellow, and calcofluor (originally blue) in cyan. White arrows show elongated bacteria. Scale bars: 500 μm (top), 50 μm (bottom).

yellow/green fluorescent appearance when observed with a FITC filter (pseudocolored in magenta for visualization purposes), suggesting the presence of polyphenolic compounds. Confocal microscopic analysis of the same nodule sections showed that, in contrast to WT nodules, BN nodules contained unevenly infected plant cells. In general, the infected plant cells of BN nodules contained spherical bacteroids, but in some cases, rod-shaped undifferentiated bacteria were also observed (Fig. 3E). These observations highlight an important role of *AeRLCK2* in nodule infection and bacterial differentiation.

AeRLCK2 physically interacts with and is phosphorylated by AeCRK

Recently, we showed that a Cysteine-rich RLK-coding gene, AeCRK, is essential for the establishment of the N-fixing symbiosis in *A. evenia* (Quilbé et al. 2021, 2022). Since RLCKs are known to interact with RLKs to mediate downstream signaling (Lin et al. 2013; Liang and Zhou 2018), we investigated the hypothesis that AeRLCK2 and AeCRK form a plasma membrane-bound complex. For this, we first examined the subcellular localization of AeCRK and AeRLCK2 in *Nicotiana benthamiana* leaves, by generating a translational fusion with the Yellow Fluorescent Protein (YFP). Transient expression of AeCRK-YFP induced cell death in *N. benthamiana* leaves 5 d after *Agrobacterium tumefaciens*-mediated transformation. In contrast, an engineered kinase-dead version (AeCRKG359E) with a mutation in the glycine-rich loop did not trigger cell death and was therefore used (Supplementary Fig. S5). The YFP fusion constructs were transiently expressed in *N. benthamiana* leaves in combination with the plasma membrane marker MtLYK3 (Klaus-Heisen et al. 2011) fused with Cyan Fluorescent Protein (CFP) (Fig. 4A). AeCRKG359E and AeRLCK2 co-localized with MtLYK3, confirming their targeting to the plasma membrane. Since, AeRLCK2 is atypical in harboring a predicted transmembrane domain (TM), we also tested an N-terminal truncated version of AeRLCK2 (AeRLCK2ΔTM-YFP). For this latter, the signal was observed in the nucleus and cytoplasmic threads, indicating that the predicted TM is important for the protein anchoring to the plasma membrane (Fig. 4A).

Next, we tested AeCRK-AeRLCK2 interactions by co-immunopurification (IP) assays. The mCherry-tagged AeCRKG359E was co-expressed with YFP-tagged AeCRKG359E, RLCK2, RLCK2ΔTM and the negative control MtLYK3-CFP in *N. benthamiana* leaves. After IP of AeCRKG359E, the co-purified proteins were detected with αGFP antibodies (Fig. 4B). AeCRKG359E-YFP and AeRLCK2-YFP were enriched 7.37-fold and 2.9-fold, respectively, compared with the negative control MtLYK3-CFP (Fig. 4B). Conversely, no significant enrichment was observed for AeRLCK2ΔTM-YFP (Fig. 4B). To assess these pairwise interactions, we performed split-luciferase assays by fusing AeCRKG359E with the C-terminal part of the luciferase (3Flag-CLuc) and the potential interactors with the N-terminal part of the luciferase (3HA-NLuc). Combination of -NLuc and -CLuc fusion proteins were co-expressed in *N. benthamiana* leaves. The corresponding bioluminescence was measured following luciferin infiltration, and the data were normalized by the expression level of the -NLuc fusion proteins (Supplementary Fig. S6). Co-expression of AeCRKG359E-CLuc with AeCRKG359E-NLuc or AeRLCK2-NLuc, but not with RLCK2ΔTM-NLuc, resulted in significantly higher bioluminescence intensities compared with MtLYK3-NLuc (Fig. 4C and Supplementary Fig. S6). Thus, these findings consistently showed that AeCRK can form homodimers and physically interact with AeRLCK2. The N-terminal domain of AeRLCK2, which confers plasma membrane localization, is essential for this interaction.

AeCRK and AeRLCK2 have typical Ser/Thr kinase domains, suggesting that their interaction may involve phosphorylation events. We therefore investigated their kinase activities. The kinase domains (KD) of AeCRK and AeRLCK2 were translationally fused to a GST-tag and expressed in *Escherichia coli*. After purification, their autophosphorylation activity was studied in vitro using radiolabelled ATP (32P-ATP). Autoradiography revealed a robust autophosphorylation activity for $AeCRK^{KD}$, whereas $AeRLCK2^{KD}$ was much less efficient (Supplementary Fig. S7). The $AeRLCK2^{KD\text{-}G110E}$ mutant, containing a mutation in the glycine-rich loop, found in *rlck2-6*, failed to incorporate 32P-ATP indicating a lack of kinase activity. Transphosphorylation studies showed that $AeCRK^{KD}$ phosphorylated the kinase-dead $AeRLCK2^{KD\text{-}G110E}$ but not free GST (Supplementary Fig. S7). These results were confirmed by *in planta* experiments with the full-length YFP-tagged proteins transiently expressed in *N. benthamiana* leaves. After IP, the phosphorylation status of the proteins was assessed using an antibody that recognizes phosphorylated serine, threonine, and tyrosine residues (Fig. 4D). AeCRK was highly phosphorylated whereas $AeCRK^{G359E}$ showed either no or low levels of phosphorylation. Surprisingly, no phosphorylation was observed for AeRLCK2 in *planta*. To investigate the possibility of trans-phosphorylation, AeCRK-YFP was co-expressed with AeRLCK2-YFP or $AeRLCK2^{G110E}$-YFP. In both cases, AeRLCK2 was phosphorylated, whereas this was not observed when using the $AeCRK^{G359E}$ version (Fig. 4D). Finally, the phosphorylation sites of AeRLCK2 targeted by the kinase activity of AeCRK were searched by comparative LC-MS/MS analysis of *in planta* immunopurified AeRLCK2 produced alone or together with AeCRK or $AeCRK^{G359E}$. Five phosphorylation sites, corresponding to 3 threonines (T66, T90 and T106) and 2 serines (S133 and S321) were identified in the cytoplasmic region of AeRLCK2 specifically in the presence of AeCRK (Supplementary Figs. S8 and S9). Consistently, AeCRK transphosphorylation of AeRLCK2 was also found using antibodies that recognize only phosphorylated threonine residues (Supplementary Fig. S8). To determine whether the AeCRK-mediated phosphorylation of AeRLCK2 is important for its function in nodulation, a phospho-silent version (all 5 sites were mutated to Ala—5A) was generated. YFP-tagged AeRLCK2 and AeRLCK2-5A were expressed under the control of *pLjUb* into the *rlck2-11* mutant via *A. rhizogenes*. Following inoculation with *Bradyrhizobium* ORS278, the *rlck2-11* plants expressing AeRLCK2-5A showed a partially stunt plant development and reduced nodule formation compared with plants expressing WT AeRLCK2, although the 2 AeRLCK2 forms showed similar levels of expression (Supplementary Fig. S10). Taken together, these results demonstrated that AeCRK and AeRLCK2 have distinct kinase activities, that AeCRK transphosphorylate AeRLCK2 on specific residues, and that these phosphosites contribute to AeRLCK2 function in nodulation.

AeRLCK2 arose from a duplication of a mycorrhiza-conserved gene in *Aeschynomene*

Since *AeRLCK2* is tandemly organized with *AeRLCK1* in the *A. evenia* genome, we investigated whether this *RLCK* gene tandem is present in other legumes. Synteny analysis based on genome sequence comparisons revealed the presence of a single *RLCK* homolog at the same locus in the analyzed legume species (Supplementary Fig. S11). To specify the relationships between *AeRLCK1*, *AeRLCK2* and *RLCK* homologs, we analysed the genome sequences of 15 legume species (13 Papilionoideae and 2 Caesalpinoideae) and 3 nonlegume species (Supplementary Data Set 1). We also included in this analysis RNAseq data from *Aeschynomene afraspera*, a close relative of *A. evenia* that uses a Nod-dependent symbiosis (Bonaldi et al. 2011) (Supplementary Table S5). This search retrieved *RLCK* homologs for each analysed plant species except *Arabidopsis thaliana* and lupin sp, 2 species unable to form AM, consistently with previous phylogenomic studies that predicted their conservation for AM (Supplementary Table S6) (Bravo et al. 2016). In rice and *L. japonicus*, the homologous genes *OsRLCK171*, *LjAMK8* and *LjAMK24* were demonstrated to be essential for AM (Leng et al. 2023). Phylogenetic

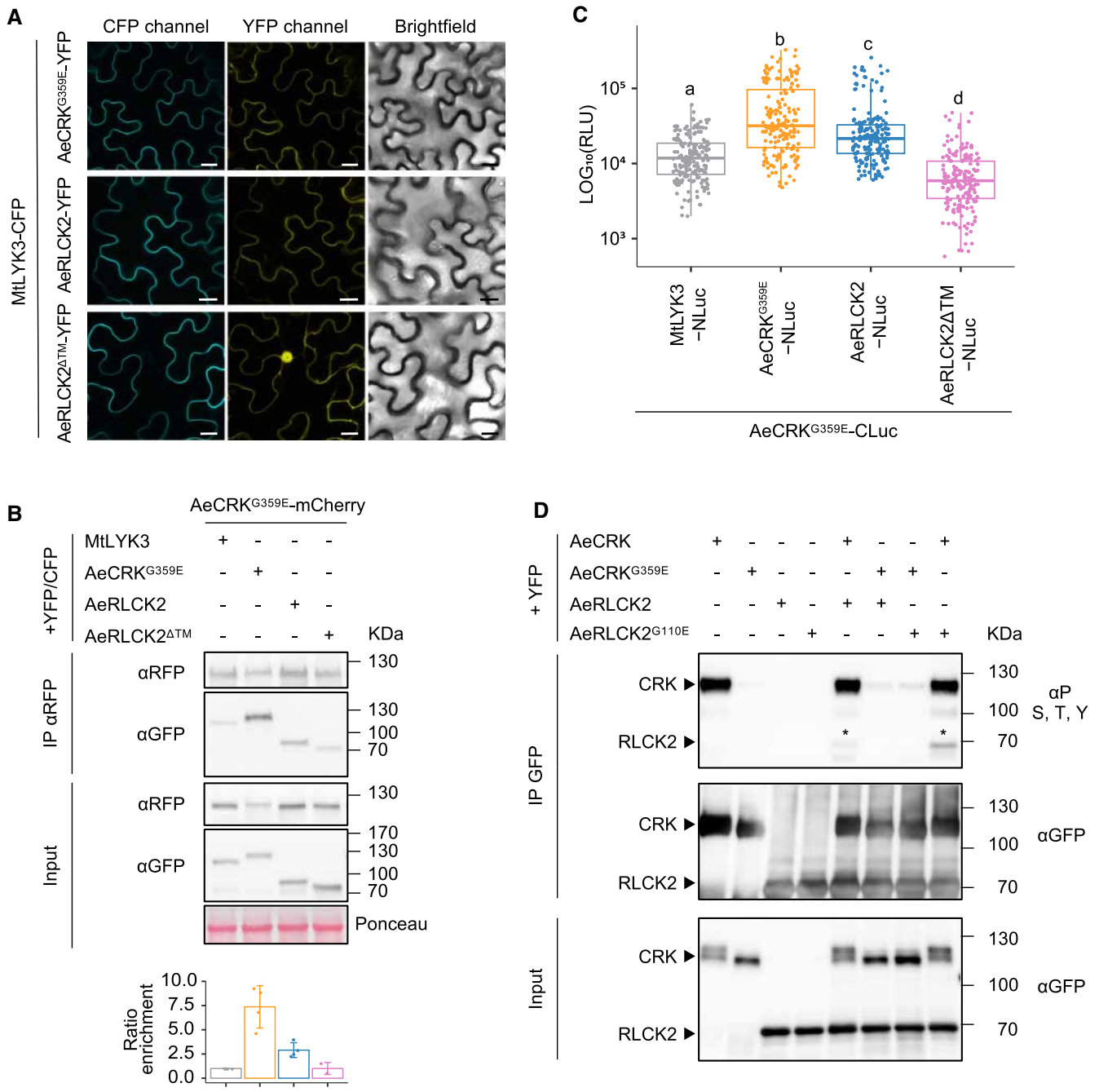

Figure 4. AeRLCK2-AeCRK interaction and kinase assays. **A)** Confocal microscopy observations of *Nicotiana benthamiana* leaf cells showing plasma membrane localization of AeCRK^{G359E}-YFP, AeRLCK2-YFP, and nucleo-cytoplasmic distribution of the truncated transmembrane version of RLCK2 (AeRLCK2$^{\Delta TM}$). MtLYK3-CFP (Cyan FP) was used as a plasma membrane marker. Scale bar: 20 μm. **B)** Co-immunoprecipitation assay showing interaction of AeCRK^{G359E}-mCherry with AeCRK^{G359E}-YFP and AeRLCK2-YFP. Proteins were immunoprecipitated (IP) with αRFP magnetic agarose beads and co-purified proteins were detected with αGFP (Green FP) antibodies (upper panel). Input (middle panel) and band intensities were calculated and normalized to the negative control MtLYK3 (bottom panel, ranging from 2 to 4 biological replicates from independent experiments). Error bars represent SD, dots show biological replicates. Ponceau staining was used as loading control. **C)** Split-luciferase assay showing the interaction of AeCRK^{G359E}-CLuc with AeCRK^{G359E}-NLuc or AeRLCK2-NLuc (N/C-terminal part of the Luciferase). Boxplots represent bioluminescence intensity from 7 biological independent replicates. Dots show individual measurements. Expression levels of 3Flag-CLuc and 3HA-NLuc fusions were assessed by western blot (Supplementary Fig. S6). Bioluminescence intensities were normalized to protein expression and data were Log-transformed (Log_{10}). Letters indicate significant differences between samples, as determined by analysis of variance (Kruskal-Wallins) and post-hoc analysis (Dunn's test), $P < 0.05$. Box plots showing the median (bold segment), interquartile range (box from Q1 to Q3), minimum and maximum (whiskers), and outliers (individual points). RLU, Relative luminescence unit. **D)** Kinase activity assay showing transphosphorylation of AeRLCK2 by AeCRK in *Nicotiana benthamiana* leaf cells. Full-length YFP-tagged proteins were immunoprecipitated with αGFP magnetic agarose beads. Phosphorylation status was analyzed after SDS-PAGE and detected with anti-S, -T and -Y antibodies. Asterisks indicate the phosphorylation status of AeRLCK2-YFP (top). Input (bottom).

reconstruction, based on protein sequences, revealed that the *RLCK* homologs present in Papilionoideae legume species were distributed in 2 sister clades, 1 containing *LjAMK8* and the other 1 *LjAMK24* (Fig. 5A). These 2 clades most probably originated from the ancient whole genome duplication (WGD) in the Papilionoideae subfamily, indicating that the rice gene *OsRLCK171* is pro-ortholog of the 2

Papilionoid paralogs, *LjAMK8* and *LjAMK24*. In *A. afraspera*, *AaRLCK_O* and *AaRLCK_P* also corresponds to the paralogous Papilionoid gene pair. In contrast, the 2 *A. evenia RLCK* genes, *AeRLCK1* and *AeRLCK2*, clustered together in the clade harboring *LjAMK8* and *AaRLCK_O*, whereas the expected paralog was missing (Fig. 5A). This suggests a recent *AeRLCK1-AeRLCK2* duplication accompanied by the loss of the paralogous gene in *A. evenia*.

To clarify when these gene changes occurred in *Aeschynomene*, we searched for *RLCK* orthologs among RNAseq data previously generated from roots and nodules for 11 *Aeschynomene* species in the Nod-independent clade (Quilbé et al. 2021). We found an *AeRLCK2* ortholog for each of these species and an *AeRLCK1* ortholog only for *A. scabra*, but no putative *RLCK* paralog was detected (Fig. 5B, Supplementary Data Set 2). We completed this analysis by experimental investigation of their presence in *Aeschynomene* species (Brottier et al. 2018). To this end, we designed primers matching conserved or specific regions to *AaRLCK_O*, *AeRLCK1* or *AeRLCK2* copies and screened by PCR amplification followed by amplicon sequencing in *Aeschynomene* species and the allied species, *Soemmeringia semperflorens*. Sequences similar to *AeRLCK1* and *AeRLCK2* were identified in the 11 Nod-independent *Aeschynomene* species as for *A. evenia*, whereas a single *RLCK* sequence was recovered in the 5 Nod-dependent species as in *A. afraspera* (Fig. 5B). Thus, there is a perfect correlation between the Nod-independent symbiosis and the *RLCK* gene duplication in *Aeschynomene* legumes. Interestingly, no additional gene tandems or clusters specific to the Nod-independent *Aeschynomene* lineage could be evidenced in the set of 138 genes predicted to be required for AM (Supplementary Table S6) (Bravo et al. 2016).

To substantiate the changes associated with *AeRLCK2*, we compared the type of *RLCK* genes present in *Aeschynomene* species. Protein sequence alignment and 3D modeling showed that they have the same general structure and share a highly conserved sequence (AeRLCK2 has 86% and 80% amino acid identity with AeRLCK1 and AaRLCK_O, respectively) (Fig. 5C and Supplementary Fig. S12). However, RLCK2 proteins are shorter at both the N- and C-terminus compared with the other RLCK proteins. We next assessed the extent of gene structural variation using *AaRLCK_O* cDNA and *AeRLCK1*/*AeRLCK2* genomic sequences. Significant differences were observed in their 5′- and 3′-UTR regions as well as in their flanking exons (Supplementary Fig. S13). We also identified a sequence in the promoter region of *AeRLCK2* that is highly similar to a downstream gene, Ae01g26580 (Supplementary Fig. S14). Our interpretation is that both the ancestral *RLCK* and the downstream genes underwent a gene tandem duplication in the ancestor of the Nod-independent *Aeschynomene* species. Subsequently, complex rearrangements occurred in the promoter region and gene extremities of the *RLCK2* copy (Supplementary Fig. S14). These data indicate that the evolution by duplication of *AeRLCK2* correlates with the evolution of the Nod-independent symbiosis.

AeRLCK2 is not essential for arbuscular mycorrhiza

To determine whether *AeRLCK2* is important for AM, as its homologs in rice (*OsRLCK171*) and *L. japonicus* (*LjAMK8* and *LjAMK28*) (Leng et al. 2023), we tested 4 *rlck2* mutants together with WT plants and the *ccamk-2* mutant line. In contrast to the completely mycorrhiza-free *ccamk-2* mutant, roots of both WT and the 4 *rlck2* mutants contained fungal hyphae, arbuscules and vesicles, 6 wk after inoculation with *Rhizophagus irregularis* spores (Fig. 6A). Quantitative assessment of AM levels using the Trouvelot method further showed that the *rlck2* mutants were colonized similarly to the WT plants (Fig. 6B, Supplementary Fig. S15).

To deepen the analysis, we focused on *rlck2-11*. At 6 wpi, there was again no difference in both the frequency and intensity of colonization between the *rlck2-11* mutant and the WT line (Fig. 6B). In parallel, quantification of the fungal *RiLSU* (large risobomal subunit) and *RiGADPH* (glyceraldehyde 3-phosphate dehydrogenase) gene expressions, as markers of fungal biomass in the root tissues was performed by RT-qPCR analysis. Expression levels of these fungal genes in *rlck2-11* roots were equivalent to those in WT roots, indicating that *R. irregularis* colonization in *A. evenia* roots is not affected by mutation in *AeRLCK2* (Fig. 6C). We also determined the expression level of plant AM-induced genes, *Reduced Arbuscular Mycorrhization 1* (*AeRAM1*), *AeVPY*, *STUNTED ARBUSCULE* (*AeSTR*) and *AeSBTM1* (Subtilase gene induced during mycorrhization) (Quilbé et al. 2022) by RT-qPCR analysis in *rlck2-11*. In this mutant, the induction levels of all genes tested were similar to those in WT plants (Fig. 6C). Therefore, the *rlck2* mutants appeared to develop functional AM.

The lack of any detectable mycorrhizal phenotype could either reflect an absence of involvement in AM of *AeRLCK2*, as recently evidenced for *AeCRK* (Quilbé et al. 2022), or a potential functional redundancy with *AeRLCK1* in AM. To address these 2 possibilities, we first considered the fact that *LjAMK8*, *LjAMK24* and the functionally related *LjKIN3* are AM-induced genes in *L. japonicus* (Leng et al. 2023) to investigate whether such an upregulation of expression occurs for *A. evenia* homologs. To enable fine expression analysis, we generated RNAseq data for WT *A. evenia* inoculated or not with *R. irregularis* (Supplementary Table S7). As previously observed (Quilbé et al. 2022), the AM-marker genes *AeRAM1*, *AeVPY*, *AeSTR* and *AeSBTM1* were well induced during AM (Supplementary Fig. S16). We observed a strong induction during AM for *AeKIN3* (Ae06g09820), the putative ortholog of *LjKIN3*, whereas the induction level of *AeRLCK1* was weaker and expression of *AeRLCK2* itself appeared to be unaffected (Supplementary Fig. S16). Since measuring expression at the root level does not always allow determining cell-specific expression, we also used the *AeRLCK2* upstream region (~2.5 kb including the 5′-UTR) to examine the *AeRLCK2* expression pattern during mycorrhization. Interestingly, the transgenic hairy roots harboring the *pAeRLCK2-GUS* construct showed a clear staining in mycorrhizal cells as evidenced for *LjAMK8*, *LjAMK24* (Supplementary Fig. S17) (Leng et al. 2023). Considering that *AeRLCK2* results from a recent duplication event, this AM-related expression might either represent a reminiscent transcriptional response to AM or, alternatively, functional redundantly with *AeRLCK1*.

AeRLCK2 shows adaptations to the Nod-independent symbiosis

To question how the Nod-independent *Aeschynomene*-specific *RLCK* gene duplication may have led to the involvement of *AeRLCK2* in nodulation, we compared the functionality of *AeRLCK2* with *AeRLCK1*, the duplicated gene in *A. evenia*, and with *AaRLCK_O*, the corresponding single copy gene in *A. afraspera*. First, the 3 RLCK proteins fused to YFP were expressed in *N. benthamiana* leaves. In contrast to AeRLCK2, cell death was observed in leaves expressing AaRLCK_O and AeRLCK1, at 8 dpi (Supplementary Fig. S18A). Confocal microscopy analysis performed at 3 dpi, i.e. before the onset of cell death, suggested that both AaRLCK_O and AeRLCK1 proteins reside at the plasma membrane, akin to AeRLCK2 (Supplementary Fig. S18B). As already evidenced for AeRLCK2, AaRLCK_O and AeRLCK1 showed no autophosphorylation activity *in planta* (Supplementary Fig. S18C). In contrast, in

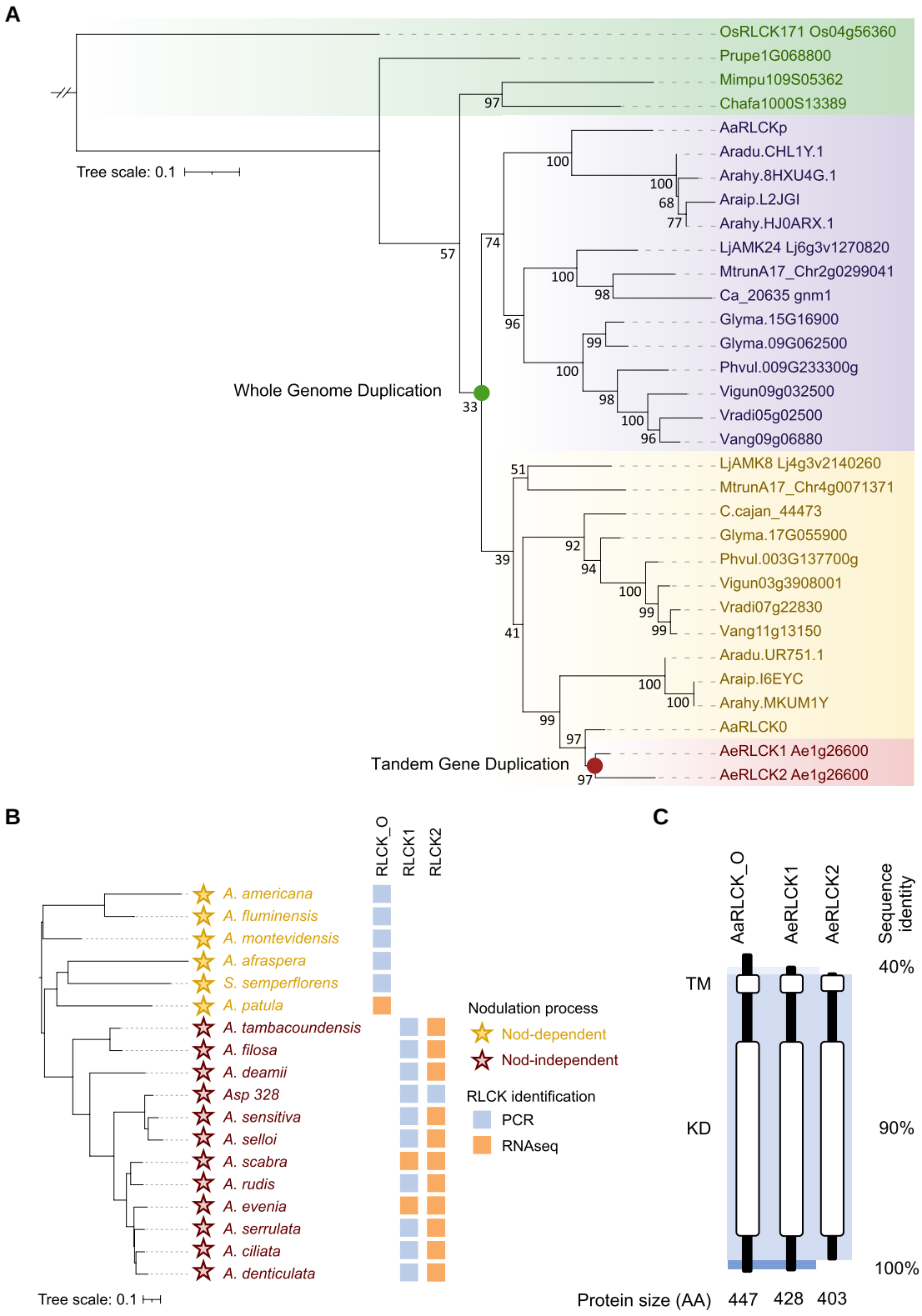

Figure 5. Phylogeny of legume *RLCK* genes and evolution in *Aeschynomene* species. **A)** Maximum likelihood (ML) phylogenetic reconstruction of the orthogroup containing AeRLCK2. Color coding indicates nonpapilionoid RLCKs (green), the 2 papilionoid RLCK clades (purple and yellow) putatively originating from the 58-MA WGD event (green dot), and the 2 RLCK copies present in *A. evenia* (red), which are derived from a recent tandem duplication (red dot). **B)** Detection of different *RLCK* gene versions in *Aeschynomene* species and the closely related species *Soemmeringia semperflorens*. The ML phylogenetic tree was constructed using concatenated *ITS* and *matK* sequences. Green stars indicate a Nod-dependent symbiosis and red stars indicate a Nod-independent symbiosis. The RLCK_O, RLCK1 and/or RLCK2 copies were identified in available RNAseq data (orange square) and by PCR amplification on genomic DNA (blue square). A and B support values were determined using 100,000 iterations of the ultrafast bootstraps approximation (UFboot). Tree scale: mutations per site. **C)** Domain structure of *Aa*RLCK_O, *Ae*RLCK1 and *Ae*RLCK2 and sequence similarities between the proteins. White bars indicate predicted domains. TM, transmembrane domain; KD, kinase domain; AA, amino acids. Intensities of blue shaded backgrounds delineate zones with different level of sequence identity. All domains are to scale.

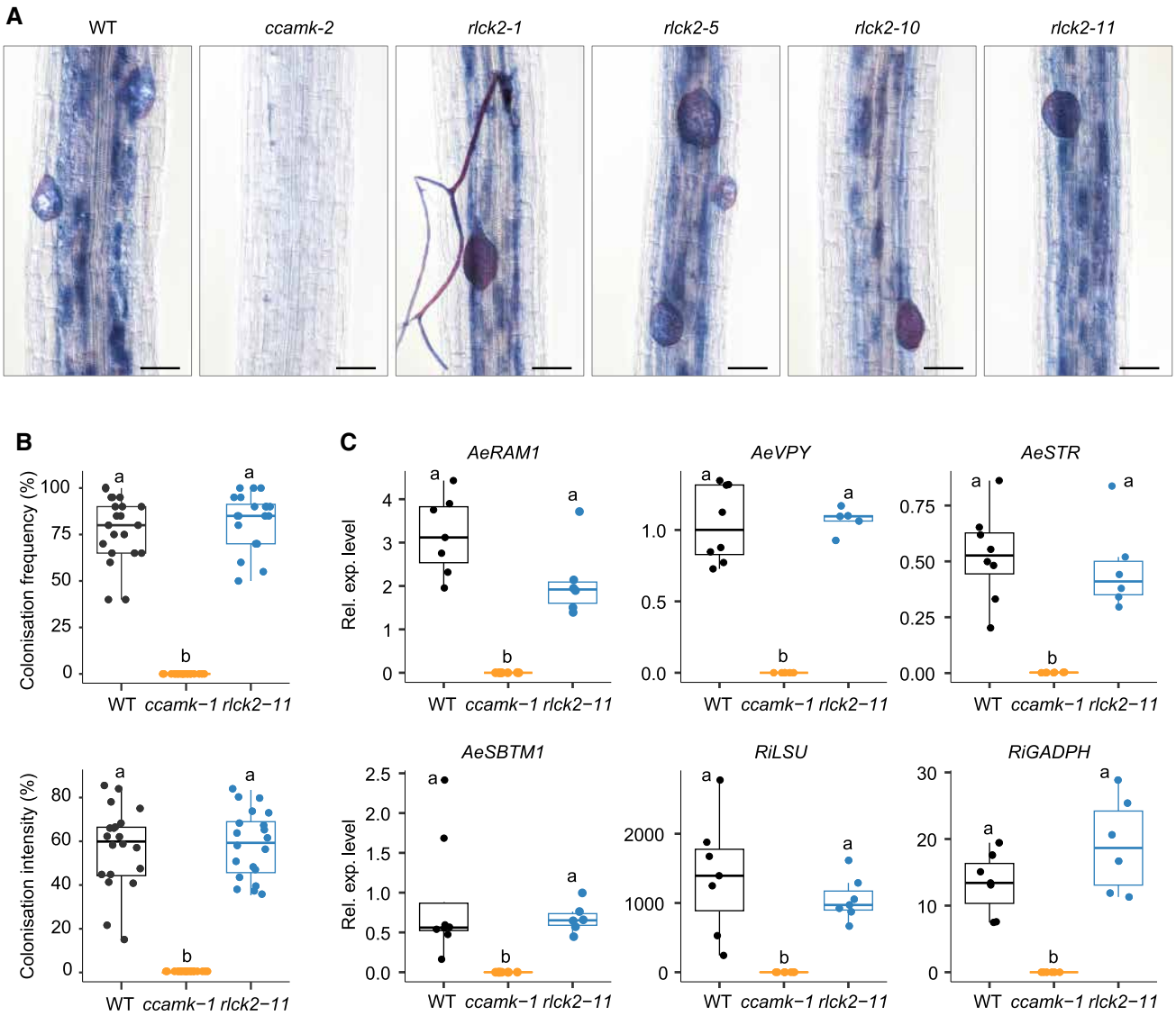

Figure 6. Arbuscular mycorrhizal (AM) root colonization in *rlck2* mutants. **A)** Microscopy images of *R. irregularis* colonization of Wild Type (WT), *ccamk-2* and *rlck2* mutants at 6 wk post-inoculation (wpi), stained with Sheaffer skrip ink. Scale bars: 50 µm. **B)** Box plots show the colonization frequency and intensity, both expressed as percentages, in 6 wpi WT, *ccamk-2* and *rlck2-11* plants. **C)** Analysis of AM-induced gene expression in WT, *ccamk-2* and *rlck2-11* plants. Relative expression levels (Rel. exp. level) of plant *AeRAM1* (Reduced Arbuscular Mycorrhization 1), *AeVPY* (VAPYRIN), *AeSTR* (STUNTED ARBUSCULE), *AeSBTM1* (subtilase gene induced during mycorrhization) and fungal *RiLSU* (large ribosomal subunit), *RiGADPH* (glyceraldehyde 3-phosphate dehydrogenase) genes were measured by RT-qPCR in roots of 6 wpi plants. The results were normalized against *AeEF1a* and *Ubiquitin*. Data presented in boxplots correspond to 4 biological replicates from independent experiments, with 5 plants per line in each replicate. Box plots show the median (bold segment), interquartile range (box from Q1 to Q3), minimum and maximum (whiskers), and outliers (individual points). Dots show individual measurements. Letters indicate significant differences between lines, as determined by analysis of variance (Kruskal-Wallis) and post-hoc analysis (Dunn's test), $P < 0.05$.

vitro kinase assays showed autophosphorylation activity for the kinase domain of the 3 RLCKs but at different levels, according to the following gradient: AaRLCK_O^{KD} > AeRLCK1^{KD} > AeRLCK2^{KD} (Supplementary Fig. S18D).

To further test whether AaRLCK_O, AeRLCK1 and AeRLCK2 are functionally equivalent, we performed cross-complementation studies. We used the *AeRLCK2* promoter to drive the expression of the *AaRLCK_O*, *AeRLCK1* and *AeRLCK2* CDS in the *rlck2-11* mutant line. Using *A. rhizogenes* root transformation and *Bradyrizobium* ORS278 inoculation, we found full complementation of the *rlck2-11* mutant phenotype with *AeRLCK2* at 3 wpi, both in terms of aerial plant development and nodule number, validating the functionality of the *AeRLCK2* promoter for nodulation (Fig. 7, A and B, Supplementary Table S8). Unexpectedly, in contrast to *AeRLCK1*, *AaRLCK_O* was also able to rescue the *rlck2-11* mutant phenotype (Fig. 7, A and B, Supplementary Table S6). Microscopy analysis of *AaRLCK_O* and *AeRLCK2* complemented roots revealed WT sized nodules with cells well-filled with bacteria (Fig. 7C). Similar results were also obtained when expressing the 3 *RLCK* genes under the constitutive Ubiquitin promoter in *rlck2-11* (Supplementary Fig. S19, Supplementary Table S8).

We next investigated whether AeRLCK2 behaves similarly to other related *RLCK* genes at the transcriptional level. Based on RNAseq data during nodulation that are available for *A. evenia* (Gully et al. 2018; Quilbé et al. 2021) and obtained in the present study for *A. afraspera* (Supplementary Table S4). *AeRLCK1* and *AeRLCK2* were found to be expressed in roots and nodules but *AeRLCK2* was at least 10-folds more expressed that *AeRLCK1* in

both organs (Fig. 8A). In contrast, *AaRLCK_O* and *AaRLCK_P* showed clear induction of their expression level during nodulation (Fig. 8A). This behavior is similar to that described in *L. japonicus* for their respective orthologs, *LjAMK8* and *LjAMK24* (Leng et al. 2023). We also analyzed the expression levels of *AeCRK* and its ortholog *AaCRK*, identified by BLAST search in the *A. afraspera* transcriptome. Expression of both *CRK* genes was found to be induced during nodulation (Fig. 8A). To better understand these contrasting expression behaviors, we monitored the spatio-temporal expression profile of *AeRLCK2* and *AeCRK* in WT roots transformed by *A. rhizogenes* with promoter-GUS fusions (Fig. 8, B and C). For *AeRLCK2*, a weak GUS staining was detected at the base of lateral roots before inoculation. After inoculation with *Bradyrhizobium* ORS278, increased GUS staining was observed at the base of lateral roots and in nodule primordia (2 and 4 dpi). When nodules emerged from the lateral root base (7 dpi), GUS staining was predominant at the nodule base and the vascular bundles of the adjacent lateral root. Finally, in mature nodules (14 dpi), GUS staining persisted at the nodule base and in the cell layers surrounding the central nitrogen-fixation zone. For *AeCRK*, no expression was detected before inoculation. At early stages of the interaction *AeCRK* expression mimicked that of *AeRLCK2* in nodule primordia (4 dpi). But then, the expression of *AeCRK* was observed in the central infected tissue of mature nodules (7 and 14 dpi). It is noteworthy that in *L. japonicus*, *LjAMK8* and *LjAMK24*, are expressed in the central infected tissue of mature nodules (Leng et al. 2023). These observations support the distinctness of the *AeRLCK2* expression pattern observed in *A. evenia*.

Discussion

A. evenia shares with a few other *Aeschynomene* species a nitrogen-fixing symbiosis with photosynthetic *Bradyrhizobium* strains that is unique among legumes in that its initiation does not depend on the perception of rhizobial Nod factors (Giraud et al. 2007). The molecular processes underlying this Nod-independent symbiosis are still largely unknown. Recently, a forward genetic approach in *A. evenia* identified signaling components that are conserved in other legumes and led to the discovery of AeCRK, a Cysteine-rich RLK (Quilbé et al. 2021, 2022). Here, using our mutant-based approach, we have identified a second symbiosis actor, AeRLCK2, which corresponds to a receptor-like cytoplasmic kinase. This is another step forward in understanding the Nod-independent symbiosis signaling pathway in *A. evenia*. The 12 *rlck2* mutants show a dual Nod-/BN phenotype, indicating a drastic reduction in the ability to initiate nodules. These mutants also lack early responses to rhizobial inoculation such as repression of ARH development, which is the first site of *Bradyrhizobium* colonization, and induction of symbiosis gene expression. In contrast to genes of the conserved symbiosis signaling pathway, for which most mutants are completely Nod-, all *rlck2* mutants occasionally develop few enlarged nodules. This singular phenotype appears to be inherent to mutations in *AeRLCK2* but it remains to be clarified whether the presence of BN nodules indicates a nontotal genetic penetrance for *AeRLCK2* [as for *NOOT* in *M. truncatula* (Couzigou et al. 2012)], the existence of a partial functional redundancy, but not with *AeRLCK1* because this latter does not complement a *rlck2* mutant, or a function that is distinct from the conserved symbiosis signaling pathway [*e.g.* the infection receptor gene *EPR3* in *L. japonicus* (Kawaharada et al. 2015)].

RLCKs lack extracellular ligand-binding domains, but they often functionally and physically associate with plasma membrane-localized RLKs to transduce intracellular signals (Lin et al. 2013; Liang and Zhou 2018). The AeRLCK2 is unusual among RLCKs in that it has a TM, but this property is conserved among its close homologs, including OsRLCK171, LjAMK8 and LjAMK24 (Vij et al. 2008; Leng et al. 2023). This TM is essential for its localization at the plasma membrane. Although its cytoplasmic domain corresponds to a typical Ser/Thr kinase, this activity was weak under in vitro conditions and not detected *in planta*. It cannot be ruled out that AeRLCK2 has a kinase activity *in planta* that was not detectable with the antibodies used. But it is also possible that some specific conditions [*e.g.* the RLCK BIK1 is activated by phosphorylation when bacterial flg22 binds to the FLS2-BAK1 complex in *A. thaliana* (Lee et al. 2017)] or the presence of interacting partners [*e.g.* several RLCKs have been shown to be strongly and specifically activated by Rop GTPases in *A. thaliana* and *M. truncatula* (Molendijk et al. 2008; Dorjgotov et al. 2009)] may be required for AeRLCK2 kinase activity. Protein-protein interaction assays revealed the association of AeRLCK2 and AeCRK in vitro and in vivo. In contrast to AeRLCK2, AeCRK showed a strong kinase activity and was able to trans-phosphorylate AeRLCK2 both in vitro and in vivo. This interaction is reminiscent of that between CRK36 and the RLCK BIK1, which is part of the FLS2-BAK1 receptor complex that perceive bacterial flg22 in *A. thaliana* (Lee et al. 2017). When activated, CRK36 increases BIK1 phosphorylation, leading to increased flg22 signaling and immunity. The AeRLCK2 residues phosphorylated by AeCRK were identified and shown to be important for AeRLCK2 function in nodulation. Additionally, the biological relevance of the AeCRK-RLCK interaction is supported by the expression of both *AeCRK* and *AeRLCK2* in nodule primordia infected by *Bradyrhizobium*, as observed using promoter-driven GUS reporters. Nevertheless, their tissular expression patterns are distinct under nonsymbiotic conditions and in mature nodules. Furthermore, the nodulation phenotypes of the *crk* and *rlck2* mutants both include early blocks in symbiosis establishment, although these blocks are different (Quilbé et al. 2021, 2022). A likely explanation is that AeCRK and AeRLCK2 have overlapping but not identical functions during symbiosis. Therefore, we hypothesize that they have other interacting partners to form 1 or more receptor complexes that mediate the Nod-independent symbiosis.

Many RLCKs have been characterized for their involvement in plant development, abiotic stress or immune responses (Lin et al. 2013; Liang and Zhou 2018). However, this analysis is very *A. thaliana*-centered, leaving out RLCKs that have no equivalent in this model plant (Vij et al. 2008). This is the case for the OsRLCK171/LjAMK8/LjAMK24 orthogroup to which AeRLCK1/AeRLCK2 belongs and for which a role in AM has only recently been uncovered (Leng et al. 2023). In *L. japonicus*, LjAMK8 and LjAMK24 interact with the RLK KIN3 and their counterparts in rice, OsRLCK171 and OsARK1, form a similar receptor complex, suggesting that this receptor complex has been evolutionarily conserved in plants for AM (Leng et al. 2023). Additionally, the expression of *LjAMK8* and *LjAMK24* in nodules suggests that they also play a role in the rhizobial symbiosis, but this remains to be confirmed (Leng et al. 2023). In *A. evenia*, what is clear is that, on 1 hand, *AeRLCK2* is expressed during AM while not essential and, on the other hand, this gene is crucial for nodulation. Additionally, *AeRLCK2* results from a tandem gene duplication event that is specific to the Nod-independent lineage within the genus *Aeschynomene*. In the duplicate *RLCK* genes, *AeRLCK1* is structurally conserved and *AeRLCK2* is more divergent, the latter having an unusual promoter sequence. This gene duplication and divergence may have facilitated the acquisition of the

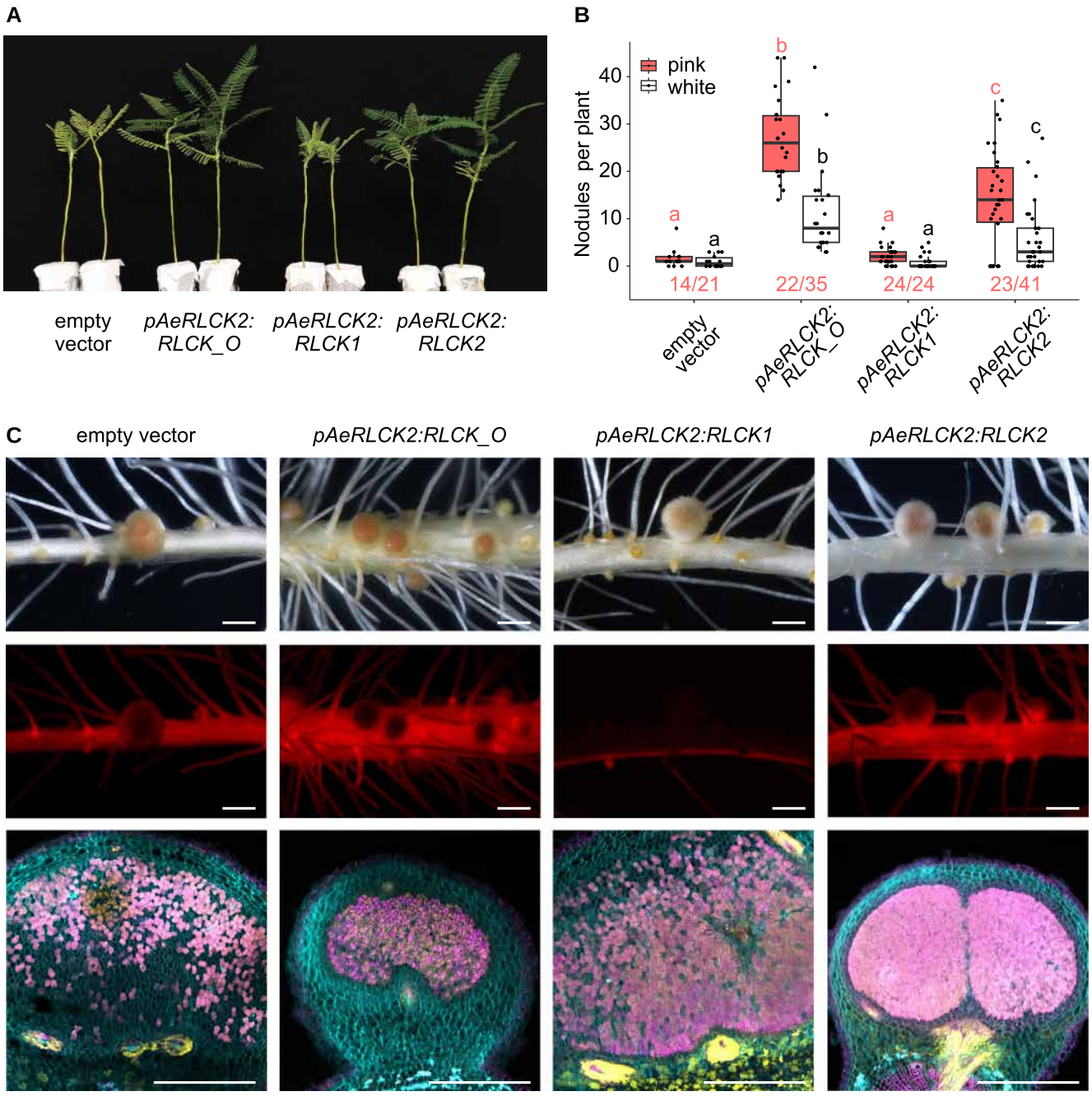

Figure 7. *A. evenia rlck2* mutant cross-complementation of root nodulation. Hairy roots of *A. evenia rlck2-11* plants were transformed with the empty vector (EV) containing the DsRed marker, or the same vector containing *pAeRLCK2:RLCK0*, *pAeRLCK2:RLCK1* or *pAeRLCK2:RLCK2* and their nodulation phenotype was evaluated 21 dpi with *Bradyrhizobium* ORS278. Observations were made on 2 biological replicates from independent experiments. Representative root nodulation phenotypes are shown here and detailed in Supplementary Table S8. **A)** Plant aerial phenotype. **B)** Number of pink and white nodules formed on plants expressing the indicated constructs. Dots represent individual plants. Red numbers below the boxplots indicate the number of plants with pink nodules, relative to the total number of transformed plants. Letters indicate significant differences between constructs, as determined by analysis of variance (Kruskal-Wallis) and post-hoc analysis (Dunn's test), $P < 0.05$. Box plots showing the median (bold segment), interquartile range (box from Q1 to Q3), minimum and maximum (whiskers), and outliers (individual points). **C)** Nodule analysis on *rlck2-11* roots transformed with the indicated constructs. Top and middle panels: microscopy observations of whole nodules under brightfield and red fluorescence using a DsRed filter, respectively. Bottom panels: cross-sections of nodules stained with SYTO 9, propidium iodide and calcofluor, and observed with a confocal microscope. For visualization purposes, SYTO 9 (originally green) was pseudocolored in magenta, propidium iodide (originally red) in yellow, and calcofluor (originally blue) in cyan. Scale bars: 1 mm (top and middle panels), 0.5 mm (bottom panel).

Nod-independent signaling. *AeRLCK1* failed to complement a *rlck2* mutant in *A. evenia*, indicating that it is functionally divergent from *AeRLCK2*. However, *AaRLCK_O*, the *RLCK* homolog in the Nod-dependent *A. afraspera*, was able to rescue the nodulation phenotype of *rlck2* mutant plants. This suggests that AaRLCK_O can still functionally replace AeRLCK2. Based on the available data, the expression pattern of *AeRLCK2* appears to differ from the *RLCK* homologs in *A. afraspera* and *L. japonicus* (Leng et al. 2023). But the lack of a genome sequence for *A. afraspera* currently precludes the analysis of tissular gene expression in this species. So far, it seems that the functional specialization of *AeRLCK2* is based on the evolution of promotor specificity and on divergence

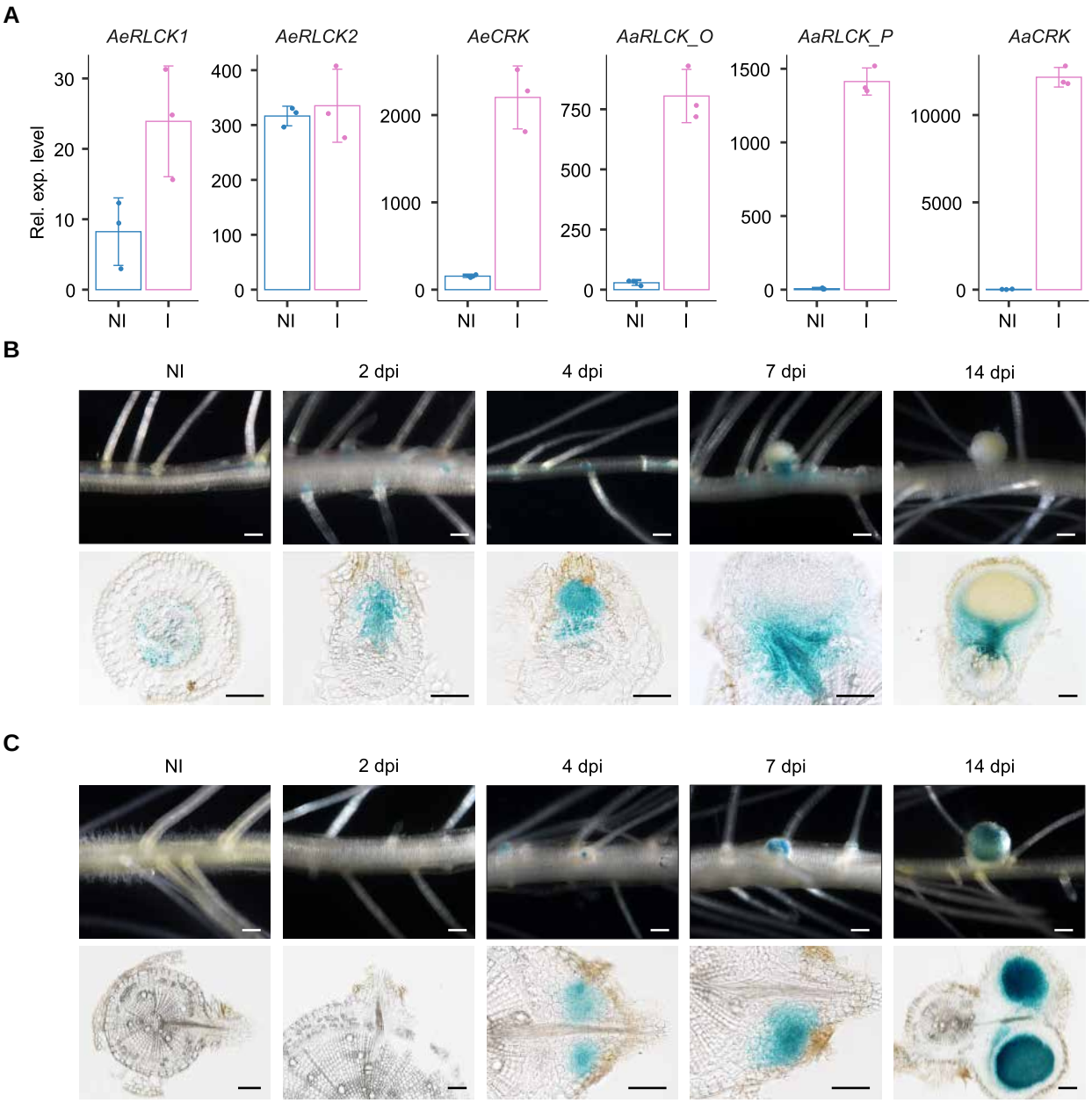

Figure 8. Expression pattern of *AeRLCK2* and comparison with other *Aeschynomene RLCK* and *CRK* genes. **A)** RNAseq-based gene expression levels of *AeRLCK1*, *AeRLCK2*, *AeCRK*, *AaRLCK_O*, *AaRLCK_P* and *AaCRK* in roots of *A. evenia* and *A. afraspera*, noninoculated (NI) and inoculated (I) with compatible *Bradyrhizobium* strains. Data correspond to 3 biological replicates from independent experiments. Error bars indicate standard deviation (SD). **B** and **C)** Histochemical localization of GUS activity in hairy roots of WT *A. evenia* transformed with **B** *pRLCK2:GUS* and **C** *pCRK:GUS* during nodulation with *Bradyrhizobium* ORS278. NI: noninoculated, dpi: days post-inoculation. Top panels: whole roots observed under a light stereomicroscope. Bottom panels: sections of roots and nodules observed by microscope. Scale bars: 1 mm (upper panels), 0.1 mm (bottom panels).

of protein function with *AeRLCK1*. Further investigations may sort out whether *AeRLCK2* represents a case of subfunctionalization or neofunctionalization, relative to *AaRLCK_O* and *AeRLCK1*.

From our work and most recent studies (Leng et al. 2023), we propose a model with proven RLCK involvements in AM through interaction of LjAMK8 and LjAMK24 with LjKIN3 in *L. japonicus* and in the Nod-independent rhizobial symbiosis through interaction of AeRLCK2 with AeCRK in *A. evenia* as well as potential roles for LjAMK8 and LjAMK24 in nodulation, and of AeRLCK2 in AM, as inferred from their tissular expression pattens (Fig. 9). A more comprehensive view of the function of *RLCK* genes in *Aeschynomene* species and the search for other occurrences of Nod-independent specific gene duplications should help us elucidate how the Nod-independent symbiosis evolved. The present advances also pave the way for the identification of additional molecular players that could be involved in the formation of receptor complex(es) with AeCRK and/or AeRLCK2 and mediate the Nod-independent symbiosis pathway in *Aeschynomene* legumes.

Materials and methods

Plant material and growth conditions

The *A. evenia* lines studied here include the CIAT22838 reference line, mutants derived from this reference line as obtained from a nodulation screen of an EMS-mutagenized population (Quilbé

et al. 2021, 2022), and the other WT accession PI225551 (Chaintreuil et al. 2018) (Supplementary Tables S1 and S2). A selection of *Aeschynomene* species, which use either a Nod-dependent or -independent symbiosis process was also selected (Brottier et al. 2018) (Supplementary Table S1). Seeds were scarified with 96% v/v sulfuric acid for 25 to 40 min with agitation, and rinsed with distilled water. Scarfied *A. evenia* seeds were incubated overnight with 0.01% (v/v) ethrel (BAYER) to induce germination (Chaintreuil et al. 2016). Plant growth during in vitro and in greenhouse conditions according to the protocols established for *Aeschynomene* sp. (Chaintreuil et al. 2016).

Genetic characterization and sequencing of nodulation mutants

Genetic analyses, consisting of genetic determinism and allelism tests, were performed on *rlck2* mutants following the methodology described previously (Quilbé et al. 2021). Without a priori gene identification by mapping-by-sequencing was performed on F2 mutant plants obtained from mutant × WT crosses (Quilbé et al. 2021). Illumina sequencing of the F2 mutant DNA pools was performed by the Norwegian Sequencing Center (CEES, Oslo, Norway) and the GeT-PlaGe platorm (INRAE, Toulouse, France). A targeted search for mutations in *AeRLCK2* was performed by PCR amplification and followed by sequencing for the de novo mutation identification in mutant lines or co-segregation analysis in F2 mutant plants (Quilbé et al. 2021). The genetic characteristics of the mutants are listed in Supplementary Table S2 and the primers used for *AeRLCK2* sequencing are listed in Supplementary Table S9.

Plant nodulation

Nodulation assays on *A. evenia* WT CIAT22838 and nodulation mutants were performed using *Bradyrhizobium* ORS278 as inoculum. To analyse the infection process, plants were inoculated with the derivative strains ORS278-GUS and ORS278-GFP (Giraud et al. 2007; Bonaldi et al. 2011).

For the in vitro nodulation test, 1-d-old seedlings were transferred to 0.8% agar-water plates at 37 °C for 24 h to achieve at least 1 cm of radicle growth. They were then transferred to covered glass tubes containing liquid buffered nodulation medium supplemented with 0.5 mM KNO3-, as described in detail (Arrighi et al. 2012). Seven days after transfer in tubes, plants were inoculated with 1 mL of bacterial culture per plant, adjusted to an OD600 = 1 using a spectrophotometer (Varian, UV-visible spectrophotometer Cary 50 scan). At 7, 10, 14, 17 and 21 dpi, the number of red and white nodules was assessed and counted using a binocular loupe. Other plant analyses were carried out on samples collected at 21 d post-inoculation (dpi). Nodule and ARH diameters were measured using ImageJ (version 2.14.0/1.54f, http://imageJ.nih.gov/ij), while the number of lateral roots per plant was evaluated using the Optimas software (version 6.1, Media Cybernitics, Silverspring, MD, USA). Nitrogenase enzyme activity is assessed by analyzing the reduction of acetylene to ethylene ARA on plants with nodules, as described (Arrighi et al. 2012).

For greenhouse experiments, scarified seeds were left overnight under gentle agitation (80 rpm) to induce radicle emergence. The next day they were transplanted into plastic trays containing attapulgite (Dry Oil, US Sorbix Special). Plants were inoculated at transplantating with 150 mL of ORS278 culture (OD600 = 1) per plastic tray (50 × 40 cm, 70 to 150 plants per tray) and grown for 4 wk before root observation.

Nodulation kinetic experiments with *A. evenia* PI225551 and *A. afraspera* LSTM1 were carried out under standard in vitro culture conditions, by inoculating plants with *Bradyrhizobium* ORS285 (Giraud et al. 2007) and collecting plant material at 0, 4 and 8 dpi.

Arbuscular mycorrhiza

Mycorrhizal phenotype studies were performed by inoculating 5-d-old *A. evenia* seedlings with spores of *Rhizophagus irregularis* DAOM197198 (Agronutrition, Carbonne, France) and growing them for 6 wk as previously described (Nouwen et al. 2024). Roots were stained with Sheaffer skrip ink, and fungal colonization was assessed on 20 root fragments per plant, with 6 plants per line, using the Myco-Calc method as described (Quilbé et al. 2022). AM was analysed using a Nikon AZ100 stereomicroscope (Champigny-sur-Marne, France), and images were taken using the Nikon Advanced software.

For analysis of GUS activity in *A. evenia* hairy roots, *Plantago lanceolata* was inoculated with *Rhizophagus irregularis* DAOM197198 spores and grown for 4 wk in pots containing zeolite and watered with 1× modified Long Ashton medium (15 μM NaH_2PO_4). Plantago shoots were cut and *A. evenia* chimeric plants were transplanted into the pots and grown for 3 more weeks. GUS staining and WGA staining were performed as described in (Girardin et al. 2019).

RNA sequencing analysis and real-time quantitative PCR

RNA was extracted from root material using the RNeasy Plant Mini Kit (Qiagen), treated with DNAse I (RNAse-Free DNAse set, Qiagen) and purified using the RNeasy Min Elute Cleanup Kit (Qiagen), according to the supplier's protocol. For RNAseq analysis, RNA material was prepared in biological triplicates of 5 plants/replicate for *A. afraspera* at 0, 4 and 8 dpi with *Bradyrhizobium* ORS285, and *A. evenia* CIAT22838 inoculated or not with *R. irregularis* DAOM197198 at 6 wpi (Supplementary Tables S5 and S7; Supplementary Data Set 3). Sequencing libraries were prepared using the TruSeq Stranded mRNA Kit and Illumina sequences generated on the MGX platform (Montpellier Genomix, Institut de Genomique Fonctionnelle, Montpellier France) and the GeT-PlaGe platorm (INRAE, Toulouse, France). *A. afraspera* Illumina RNA-seq datasets were de novo assembled using DRAP (Cabau et al. 2017), and those of *A. evenia* were mapped to the *A. evenia* reference genome using nf-core/rnaseq pipeline (Patel et al. 2024). Gene expression levels were normalized using the Diane pipeline (Cassan et al. 2021). For expression analysis, root material was generated in 4 biological replicates for the *A. evenia* CIAT22838 WT line and nodulation mutants at 0, 2, 4, and 7-dpi with *Bradyrhizobium* ORS278 (3 plants/line/replicate) and at 6 wpi with *R. irregularis* DAOM197198 (5 plants/line/replicate).

RT-qPCR was performed using the Takyon SYBRMaster Mix dTTP Blue kit (Eurogentec) in a 96-well plate format and the Stratagene MX3005P thermocycler (Agilent Technologies). The amplification protocol consisted of the following cycle: 3 min at 95 °C + 40 cycles of (10 s at 95 °C + 30 s at 60 °C + 60 s at 95 °C + 30 s at 60 °C) + 30 s at 95 °C. MXPro software was used to analyze the results based on the cycle threshold (CT) value. The gene expression level was obtained using the formula N = 10 ((CT-b)/a)—where a and b vary according to the efficiency of each primer pair. The housekeeping genes *AeEF1α* and *AeUbi* were used for subsequent normalization of expression levels. Primers used for quantification of gene expression are listed in Supplementary Table S10.

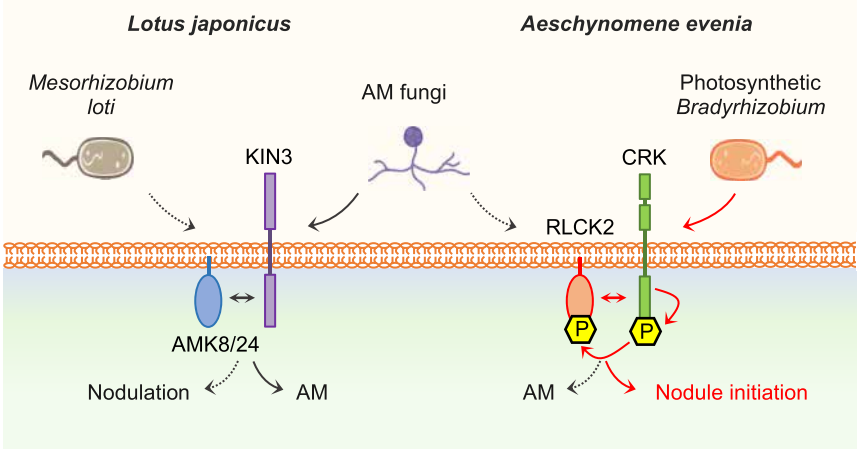

Figure 9. Model of RLCK functions in arbuscular mycorrhiza (AM) and Nod-independent symbiosis in legumes. During AM in *L. japonicus*, the paralogs AMK8 and AMK24 (ARBUSCULAR MYCORRHIZA-INDUCED KINASES) interact with KIN3 (KINASE 3) at the periarbuscular membrane. Autophosphorylation and transphosphorylation events in this RLCK-RLK complex are linked to mediate downstream AM responses. In contrast to *LjKIN3*, *LjAMK8* and *LjAMK24* are also expressed during nodulation; however, their putative role in the rhizobial symbiosis remains unknown. In *A. evenia*, the LjAMK24 counterpart is absent, while 2 proteins, AeRLCK1 and AeRLCK2, are closely related to LjAMK8. AeRLCK2 is expressed during AM but does not appear to be essential for this process. While the symbiotic role of AeRLCK1 is currently unknown, AeRLCK2 is central in mediating Nod-independent symbiosis with photosynthetic bradyrhizobia. One of its functions is to interact with and be phosphorylated by AeCRK at the plasma membrane, which is important for RLCK2 function in nodule initiation. The upstream signal and downstream signaling components remain to be elucidated.

Sequence collection and *in silico* gene analysis

The Ae01g26600 gene is misannotated in the *A. evenia* genome v1. Based on *A. evenia* RNAseq data, it was manually curated to delineate *AeRLCK1* and *AeRLCK2* (Supplementary File 1). Microsynteny analysis was performed using the Legume Information System with the Genome Context Viewer (https://legumeinfo.org/lis_context_viewer) to visualize the gene collinearity in syntenic regions. RLCK protein domains were identified and annotated using InterProscan (http://www.ebi.ac.uk/interpro/) and DeepTMHMM (https://dtu.biolib.com/DeepTMHMM).

AeRLCK2 homologs were identified in legume species by mining the orthogroup database generated with OrthoFinder during the previous *A. evenia* genome project (Quilbé et al. 2021). RLCK sequences were also obtained by BLASTP searches in lupin genomes where *RLCK* genes are present but not annotated and, in the *A. afraspera* transcriptome generated in this study. The dataset was completed by searching for additional RLCK proteins in *A. thaliana*, *O. sativa* and *P. persica* in the Arabidopsis Information Resource (https://www.arabidopsis.org), the Rice Genome Annotation Project (http://rice.uga.edu) and the Phytozome (https://phytozome-next.jgi.doe.gov/) databases, respectively. A total of 32 RLCK protein sequences were retrieved from a set of 18 plant species and used for phylogenetic reconstruction (Supplementary Data Set 1; Supplementary File 1). Identified homologous proteins were aligned using MAFFT v7 (Katoh et al. 2019) with the auto strategy, allowing for gapped regions. To optimize the alignments and select the most appropriate approach for Maximum Likelihood analysis, trimAL v1.4.1 was used with the automated-1 option (Capella-Gutiérrez et al. 2009). The resulting alignments were used for phylogenetic analysis using IQ-tree v2.2.0.3 (Minh et al. 2020) with the recommended best-fit model from ModelFinder (Kalyaanamoorthy et al. 2017). Support values were determined with 100,000 iterations of ultrafast bootstrap approximation (UFboot) (Hoang et al. 2018). Tree visualization and annotation was performed using iTOL v6 (Letunic and Bork 2024). The tree was rooted with the most distant *O. sativa* RLCK homolog, which served as outgroup.

For the analysis of *RLCK* copy number in the genus *Aeschynomene*, additional protein sequences were retrieved in the OrthoFinder-derived RLCK orthogroup for species with available transcriptomes (Quilbé et al. 2021). For an extended set of *Aeschynomene* species (Supplementary Data Set 2), DNA was extracted using the CTAB method and served as matrix for PCR amplication using different pairs of primers designed as general or copy-specific to amplify an *RLCK* gene fragment in *Aeschynomene* species (Supplementary Table S9). The amplicons were amplified by Sanger technology. Transcriptome and PCR-derived sequences were translated into protein sequences and aligned to AaRLCK_O, AeRLCK1 and AeRLCK2 in Multalin (http://multalin.toulouse.inra.fr/multalin/multalin.html) for comparison (Supplementary Data Set 2; Supplementary File 2). To reconstruct the phylogeny of *Aeschynomene* species, previously published nuclear *ITS* (Internal Transcribed Spacer) and chloroplast *matK* sequences (Brottier et al. 2018) were concatenated and processed using the same methods described above. The symbiosis type and the presence of the different *RLCK* gene copies were added to the species tree.

Sequence alignments and tree files are provided in Supplementary Data Set 4.

Cloning and plasmid construction

For the initial complementation assay of the *rlck2-11* mutant, the 1212 nucleotide *AeRLCK2* CDS was PCR-amplified from *A. evenia* cDNAs, and cloned into the CR8/GW/TOPO entry vector, to generate pCR8-*AeRLCK2*. It was then transferred into the pUB-GW-GFP vector via the LR reaction (Invitrogen) to generate the p*Ubi-AeRLCK2-GFP* construct, in which the *GFP* gene is used as a fluorescent marker for plant transformation.

To analyse *AeRLCK2* and *AeCRK* expression in hairy roots, the *AeRLCK2* promoter (2,537 pb upstream of the start codon) and the AeCRK promoter (1,381 pb upstream of the start codon) were synthesized and cloned into the Puc57-BSAI-free plasmid by GeneCust (www.genecust.com) (Supplementary File 3). The cloned promoters were subsequently fused to the *GUS* gene by

GoldenGate cloning, using the pCambia2200-DsRed vector (Fliegmann et al. 2016).

For complementation tests of the *rlck2-11* mutant with the phospho-silent version of *AeRLCK2* (*AeRLCK2*^{5A}), the corresponding CDS was synthesized and cloned into the Puc57-BSAI-free plasmid by GeneCust (Supplementary File 3). The *AeRLCK2* and *AeRLCK2*^{5A} were subsequently cloned in translational fusion to the *YFP* gene downstream of the p*LjUb* promoter by GoldenGate cloning, using the pCambia2200-DsRed vector (Fliegmann et al. 2016).

For cross-complementation tests on the *rlck2-11* mutant, the *AaRLCK_O*, *AeRLCK1* and *AeRLCK2* CDS were PCR-amplified from *A. afraspera* and *A. evenia* cDNAs, respectively, and cloned in the pMiniT 2.0 vector (NEB PCR Cloning Kit, New England Biolabs). Using the GoldenGate cloning method (Fliegmann et al. 2016), they were placed downstream of both the p*LjUb* and the p*AeRLCK2* promoters in the pCambia2200-DsRed vector, where the *DsRed* gene is used as a fluorescent marker for plant transformation.

For gene expression in *N. benthamiana* leaves and subsequent protein production, the *AaRLCK_O*, *AeRLCK1*, *AeRLCK2* and *AeCRK* CDS without ending stop codon were cloned into pGEMT plasmids. An *AeRLCK2*ΔTM version, corresponding to the AeRLCK2 protein without the N-ter TM was also produced. Golden gate assembly was performed in the pCambia2200 vector as described (Fliegmann et al. 2016).

For the split-luciferase assay, the N-terminal and C-terminal parts of the luciferase were fused with a triple hemaglutin3HA or a triple Flag (3Flag) tag, respectively, and flanked by compatible Golden gate extensions. The luciferase modules were synthetized by Azenta (www.azenta.com), and assembled with the CDS to be tested as targets and placed under the control of the p*LjUb* promoter in a modified pCambia2200 vector by GoldenGate cloning (Fliegmann et al. 2016).

For in vitro assays, the predicted kinase domain of AeRLCK2 (G74—S403) was amplified by PCR and cloned into a modified pCDFDuet-1 vector (Novagen), as described for the cloning of AeCRK kinase (Quilbé et al. 2022). Site-directed mutagenesis was performed to generate the AeCRK$^{KD\text{-}G359E}$ (inactive kinase mutation) and AeRLCK2$^{KD\text{-}G110E}$ (*rlck2-6* mutant allele mutation) variants using the Q5 Site-Directed Mutagenesis Kit (New England Biolabs). The kinase domains of AaRLCK_O (E99 to Q447) and AeRLCK1 (E83 to F428) were amplified by PCR and cloned into pET-41a (Novagen) plasmid by restriction-ligation.

All PCR amplifications were performed using high-fidelity DNA polymerase Taq Phusion (New England Biolabs) or PrimeSTAR Max DNA polymerase (Takara). All constructs were verified by restriction enzyme digestion followed by sequencing with the Sanger technology. Different *E. coli* strains, Dh10b (ThermoFisher Scientific), TOP10 (ThermoFisher Scientific), XL10-Gold (Agilent) and Rosetta/DE3 (Novagen Sigma-Aldrich) were used for molecular cloning or protein expression. Final constructs were electroporated into *Agrobacterium rhizogenes* Arqua1 cells for transformation of *A. evenia* hairy roots (Quilbé et al. 2021) or into *Agrobacterium tumefaciens* LBA4404 VirGN54D for transient expression in *Nicotiana benthamiana* leaves (Voinnet et al. 2003). All primers are listed in Supplementary Table S9.

Analysis of promoter-GUS and complementation of *A. evenia* transformed hairy roots

Agrobacterium rhizogenes Arqua1 strains carrying the indicated constructs were used to transform roots of WT *A. evenia* CIAT22838 line and *rlck2-11* mutant. Transformation of hairy roots was carried out as previously described (Quilbé et al. 2021). Briefly, 2-d-old seedlings with freshly cut radicles were directly inoculated with *A. rhizogenes* Arqua1 carrying the desired plasmid. They were grown on solid MS (Murashige and Skoog basal salt mixture) at 20 °C in the dark for 5 d and then transferred to solid MS medium containing 300 μg/mL cefotaxime. Plants bearing transgenic hairy roots were transferred to covered glass tubes containing liquid buffered nodulation media supplemented with 1 mM $KNO3^{-}$. Seven days after transfer, plants were cultivated and inoculated with *Bradyrhizobium* ORS278 according standard procedures. The *A. evenia* WT hairy roots transformed with p*AeRLCK2:GUS* and p*AeCRK:GUS* were stained with X-Gluc to vizualize gene expression at the indicated time-points. For the *A. evenia rlck2-11* complementation assays, nodule formation was monitored 21 d after inoculation.

Macroscopic and microscopic observations

All root samples from noninoculated and inoculated roots were visually inspected using a Nikon AZ100 stereomicroscope (Champigny-sur-Marne, France) and imaged using the Nikon Advanced software. Where needed, fresh 42 micron thick section of roots and nodules were made using a Leica VT1000s vibratome. For bacterial infection analysis (ORS278-GUS) and promoter activity studies, Whole plant roots or sectioned samples were stained with X-Gluc (Fabre et al. 2015) and then analysed using a Nikon macroscope or microscope. Gene expression was observed at different time-points in both young and older noninoculated plants, and at 2, 4, 7, 10, 14 and 21 dpi for plants inoculated with ORS278. To investigate bacterial infection with ORS278, freshly sectioned nodules were incubated with the live/dead reagent (Syto9/propidium iodide) and then stained with calcofluor white, as previously described (Nouwen et al. 2024). Samples were analysed using a confocal laser-scanning microscope (Carl Zeiss LSM 700, Jena, Germany). Calcofluor was excited at 405 nm and emitted light collected between within 405 to 470 nm, while SYTO 9 and propidium iodide were excited at 488 and 555 nm, respectively, with emissions collected between 490 to 522 nm and 555 to 700 nm. Images were acquired using the ZEN 2008 software (Zeiss, Oberkochen, Germany).

Subcellular localization in *Nicotiana benthamiana* leaves

N. benthamiana plants were grown in a controlled environment chamber under the following conditions: 19 to 21 °C with a 16 h light/8 h dark photoperiod. Four-week-old plants were used for *A. tumefaciens*-mediated transformation to achieve transient protein expression. *A. tumefaciens LBA4404 VirGN54D* strains containing the desired constructs were grown overnight in liquid LB medium, centrifuged at 7,000 g for 3 min, and washed twice with agroinfiltration buffer (10 mM MES-KOH pH 5.6, 10 mM MgCl2 and 150 μM acetosyringone). The optical density (OD600) was measured and adjusted to OD600 = 0.5. *A. tumefaciens* expressing the P19 protein (RNA silencing suppressor) was added to the *A. tumefaciens* solutions (OD600 = 0.2) to enhance protein expression (Voinnet et al. 2003). *N. benthamiana* leaves were agroinfiltrated with a needleless syringe and leaves were harvested 3 d later. Subcellular localization was assessed 72 h after infiltration with a ×25 water immersion objective lens (confocal microscope, SPE8 Leica). MtLYK3-CFP was used as a plasma membrane marker (Klaus-Heisen et al. 2011) and co-expressed with YFP fusion

proteins. The excitation/emission filter sets for CFP and YFP were 458 nm/463 to 512 and 514 nm/525 to 580 nm, respectively.

Protein-protein interaction assays

Different construct combinations (MtLYK3-CFP, AeCRK^{G359E}-YFP, AeRLCK2-YFP, AeRLCK2ΔTM-YFP and AeCRK^{G359E}-mCherry) were agroinfiltrated into *N. benthamiana* leaves together with p19. Leaf material was collected 3 d after infiltration, and proteins were extracted for co-immunoprecipitation assays as previously published (Ding et al. 2024). YFP fusion bands were quantified using Image Lab 6.0 (volume function). Enrichment ratios (signal IP αGFP/signal input αGFP) were normalized using the negative control MtLYK3-CFP (signal αRFP).

The split-luciferase assay was performed as previously described (Landry et al. 2023). Briefly, *A. tumefaciens LBA4404 VirGN54D* strains containing the indicated NLuc and CLuc plasmids were co-infiltrated into 4-week-old *N. benthamiana* leaves. After 72 h, 4 mm leaf discs were placed in a 96-well plate, washed twice with water, and incubated with 1 mM luciferin substrate (Xenolight, PerkinElmer). Light emission was then quantified using a luminometer (VICTOR Nivo, PerkinElmer). Protein expression levels were assessed from 7 mm leaf discs, which were previously used to quantify luciferase activity. After protein extraction and Western blotting, 3HA-NLuc fusion bands were quantified using the volume function in Image Lab 6.0. The corresponding data were used to calculate a ratio normalized to the negative control AeCRK^{G359E}-Cluc/MtLYK3-Nluc. Raw data were normalized using the previously calculated ratio to account for variation in protein expression.

For Western blotting, leaf samples were ground in liquid nitrogen using a Retsch mixer mill (MM400). Proteins were solubilized in Laemmli buffer, heat-denatured at 95 °C for 5 min and separated by SDS-PAGE on home-made gels or 4% to 15% precast polyacrylamide gel (Bio-rad).

Proteins were transferred to a nitrocellulose membrane using the Transblot-Turbo system (Bio-rad) according to the manufacturer's instructions. The nitrocellulose membrane was blocked for 1 h at RT (or overnight at 4 °C) with 5% nonfat milk or 3% BSA solution in Tris-saline buffer (TBS) supplemented with 0.1% Tween-20 (TBS-T). As a loading control, Ponceau S staining solution was used to visualize Rubisco protein. The membrane was then incubated with the appropriate antibodies for 1 h at RT (or overnight at 4 °C). The following antibodies were used for protein biochemistry experiments: αHA-Hrp (12013819001, Roche, 1/5000), αFlag-Hrp (A8592, Sigma-Aldrich, 1/5000), αRabbit-Hrp (12–348, Millipore, 1/20000), αGFP (11814460001, Roche, 1/3000), goat αMouse-Hrp (1706516, Bio-Rad, 1/10000), rabbit αRFP (1/5000) (Lefebvre et al. 2012). Hrp bioluminescence was detected using Clarity Western ECL substrate (Bio-rad) and observed using the ChemiDoc imager (Bio-rad).

In vitro and *in planta* phosphorylation assays

For in vitro assays, sequences coding AeRLCK2^{KD} and its mutant form AeRLCK2$^{KD\text{-}G110E}$, AeCRK^{KD} and its mutated form AeCRK$^{KD\text{-}G359E}$, AaRLCK_O^{KD} and AeRLCK1^{KD}, were expressed in *E. coli* as GST fusion proteins at 16 °C. Proteins were purified using Glutathione-agarose beads (Amersham Biosciences) as described (Klaus-Heisen et al. 2011). AeCRK^{KD} was released from the resin using PreScission Protease (GE27-0843-01, Sigma-Aldrich, Germany). For radiolabeled kinase assays, proteins were incubated for 30 min at 30 °C in 10 mM HEPES-HCl pH 7.4 containing 5 mM $MgCl_2$, 5 mM $MnCl_2$, 20 μM ATP and 5 mCi 32P-ATP. Reactions were analysed by SDS-PAGE, followed by Coomassie staining and Phosphor imaging. Alternatively, proteins were incubated in the same buffer containing 40 μm ATP for 30 min at 30 °C. Reactions were analysed by SDS-PAGE, transferred to a nitrocellulose membrane and αPhospho-ser-thr-tyr (61-8300, Invitrogen, 1/333), followed by αRabbit-Hrp.

For *in planta* phosphorylation assays, proteins were extracted (w/v, 0.2/1) with protein extraction buffer [50 mM Tris-HCl 7.5, 150 mM NaCl, 10 mM EDTA, Triton X-100 1%, DTT 2 mM, supplemented with protease inhibitor cocktail (Sigma) and phosphatase inhibitor cocktail 3 (Sigma)]. Proteins were solubilized for 30 min at 4 °C and then centrifuged at 20,000 g for 5 min at 4 °C. The supernatant was filtered through Miracloth and incubated for 2 h at 4 °C with αGFP magnetic agarose beads (Chromotek). The beads were washed 3 times with protein extraction buffer. Proteins were solubilized in Laemmli 2× buffer, heat denaturated at 95 °C and subsequently separated by SDS-PAGE. The phosphorylation status was assessed using αPhospho-ser-thr-tyr or αPhospho-thr (1/2000, Zymed), followed by αRabbit-Hrp. Identification of phosphorylated sites by LC-MS/MS analysis was performed as described in detail in Supplementary Note S1.

Statistical analysis and graphs

Data analysis and visualization were performed using R with the ggplot2 package (Wickham 2016; R Core team et al. 2020). The Kruskal-Wallis test, followed by Dunn's post-hoc test for multiple comparisons, was used for all statistical analysis (Kruskal and Wallis 1952; Dunn 1964). All source data and detailed statistical results are provided in Supplementary Data Set 5.

Accession numbers

Supplementary sequence information used in this article for *Aeschynomene evenia* can be found in AeschynomeneBase (https://aeschynomenebase.fr/). Gene accession numbers are *AeCCamK* (Ae08g13330), *AeCRK* (Ae05g12380), *AeEF1a* (Ae09g20140), *AeKIN3* (Ae06g09820), *AeNIN* (Ae07g00100), *AeRAM1* (Ae06g18380), *AeRLCK2* (Ae01g26600), *AeSBT* (Ae05g09230), *AeSBTM1* (Ae05g09240), *AeSTR* (Ae05g35200), *AeSYMREM1* (Ae03g30480), *AeUbi* (Ae10g10900), *AeVPY* (Ae05g16930).

Acknowledgments

We thank Robin Duponnois (LSTM Laboratory, IRD) for assistance with the characterization of the *A. evenia* nodulation mutants and for kindly providing fungi spores for AM experiments. We would also like to thank Virginie Gasciolli, Céline Vicedo and Léandre Bouat (LIPME Laboratory, INRAE) for their technical assistance. Illumina sequence data were produced by the MGX platform (https://www.mgx.cnrs.fr/), the Norwegian Sequncing Center (http://www.sequencing.uio.no) and the GeT-PlaGe platform (https://get.genotoul.fr/la-plateforme/get-plage/). Computing was performed thanks to the GenoToul bioinformatics facility (http://bioinfo.genotoul.fr/). The project also benefited from the expertise of the Proteomics French Infrastructure (https://www.profiproteomics.fr/) and France-BioImaging Infrastructure (https://france-bioimaging.org/) located at the Agrobiosciences, Interactions and Biodiversity Research Federation (https://www.fraib.fr/).

Author contributions

J.-F.A. and B.L. conceived the whole project and supervised data analyses. J.Q. performed the genetic and molecular analysis of

the *rlck2* mutants, to which J.-F.A. contributed. N.H.A conducted the phenotypic characterization of the *rlck2* mutants and RT-qPCR analyses relative to the nodulation and AM tests, to which J.Q. and M.P. contributed. N.H.A., D.L., J.Q. and C.G. conducted phylogenetic and evolutionary analyses. N.H.A., J.Q. and M.R. generated molecular constructs and conducted functional experiments on *AeRLCK2*. D.L. performed the biochemical characterization of AeRLCK2 and AeCRK, to which J.C. and C.P. contributed. M.P., F.G., and D.G. produced plant material and RNA material. L.B. screened the *A. evenia* mutagenized population to isolate *rlck2* mutants. C.K. and M.R. analyzed the sequence data for the Mapping-by-Sequencing analysis of the *rlck2* mutants as well as for the RNAseq data. M.P., F.G., C.C., N.N. and E.G. contributed to different experiments and provided their assistance for the achievement of the project. N.H.A., D.L., C.V., V.G., and B.L. conducted additional in vitro kinase assays, nodulation and AM tests for the revision of the manuscript. J.F.A., N.H.A., D.L. and B.L. wrote the manuscript. N.H.A produced the figures, to which D.L. contributed. All authors critically commented on and approved the manuscript.

Supplementary data

The following materials are available in the online version of this article.

Supplementary Figure S1. Identification of *A. evenia rlck2* mutant alleles via mapping-by-sequencing.

Supplementary Figure S2. Nodulation kinetics of WT and *rlck2* mutants.

Supplementary Figure S3. ARH development in the *crk-1* mutant.

Supplementary Figure S4. Aerial phenotype of WT and *rlck2* mutants grown in in vitro chambers.

Supplementary Figure S5. AeCRK induces cell death in *Nicotiana benthamiana* leaves.

Supplementary Figure S6. Expression of 3HA-NLuc fusion proteins.

Supplementary Figure S7. AeCRK kinase activity and AeRLCK2 transphosphorylation in vitro.

Supplementary Figure S8. The phosphorylation sites of AeRLCK2 specifically targeted by AeCRK.

Supplementary Figure S9. MS/MS fragmentation spectra supporting Supplementary Fig. S8.

Supplementary Figure S10. *Aeschynomene evenia rlck2-11* mutant complementation of root nodulation using a phospho-silent version.

Supplementary Figure S11. Microsynteny analysis of the *AeRLCK2* locus.

Supplementary Figure S12. Alignment and structure of *Aeschynomene* RLKC proteins.

Supplementary Figure S13. Comparison of gene structure between *AaRLCK_O*, *AeRLCK1* and *AeRLCK2*.

Supplementary Figure S14. Model of gene duplication at the *AeRLCK2* locus.

Supplementary Figure S15. Mycorrhizal phenotype of the *rlck2* mutants.

Supplementary Figure S16. Gene expression levels during AM in *Aeschynomene evenia*.

Supplementary Figure S17. Expression of *AeRLCK2* in arbuscule-containing cells.

Supplementary Figure S18. Comparative analysis of *AeRLCK1* and *AaRLCK_O*.

Supplementary Figure S19. *Aeschynomene evenia rlck2* mutant trans-complementation of root nodulation using p*LjUb*.

Supplementary Table S1. *Aeschynomene* species used in this study.

Supplementary Table S2. Phenotypic, genetic and molecular data on the *Aeschynomene evenia* nodulation mutants.

Supplementary Table S3. Allelism analysis of the *Aeschynomene evenia rlck2* mutants.

Supplementary Table S4. Functional complementation test for nodulation with *AeRLCK2*.

Supplementary Table S5. Summary of Illumina transcriptome sequencing and assembly for *Aeschynomene afraspera*.

Supplementary Table S6. Summary of Illumina transcriptome sequencing for *Aeschynomene evenia* CIAT22838.

Supplementary Table S7. Analysis of the list of 138 AMS conserved genes.

Supplementary Table S8. Nodulation data for the cross-complementation tests of *rlck2* mutant.

Supplementary Table S9. Primer sequences used for PCR amplification, cloning and site-directed mutagenesis.

Supplementary Table S10. List of genes with the primers used for RT-qPCR analysis.

Supplementary Data Set 1. Annotation resources for plant genomes used in this study.

Supplementary Data Set 2. Annotation resources for *Aeschynomene* species used in this study.

Supplementary Data Set 3. Sequence data for *Aeschynomene* spp.

Supplementary Data Set 4. Sequence alignments and tree files used in Fig. 5, A and B.

Supplementary Data Set 5. Source data and statistical results.

Supplementary File 1. *RLCK* sequences used for the phylogeny presented in Fig. 5A.

Supplementary File 2. *RLCK* sequences used for the analysis presented in Fig. 5B.

Supplementary File 3. Sequences synthesized for *AeRLCK2* and *AeCRK*.

Supplementary Note S1. Identification of AeRLCK2 phosphorylation sites.

Funding

This study was supported by 4 grants from the French National Research Agency (ANR-SymWay-21-CE20-0011-01, ANR-DUALITY-20-CE20-0017, ANR-AeschyNod-14-CE19-0005-01 and ANR-BugsInaCell-13-BSV7-0013-02).

Conflict of interest statement. None declared.

Data availability

The data underlying this article are available in the article and in its online supplementary material.

References

Arrighi JF, Cartieaux F, Brown SC, Rodier-Goud M, Boursot M, Fardoux J, Patrel D, Gully D, Fabre S, Chaintreuil C, et al. *Aeschynomene evenia*, a model plant for studying the molecular genetics of the Nod-independent rhizobium-legume symbiosis. *Mol Plant Microbe Interact*. 2012:25(7):851–861. https://doi.org/10.1094/MPMI-02-12-0045-TA

Bonaldi K, Gargani D, Prin Y, Fardoux J, Gully D, Nouwen N, Goormachtig S, Giraud E. Nodulation of *Aeschynomene afraspera*

and *A. indica* by photosynthetic *Bradyrhizobium* sp. strain ORS285: the nod-dependent versus the nod-independent symbiotic interaction. *Mol Plant Microbe Interact*. 2011:24(11):1359–1371. https://doi.org/10.1094/MPMI-04-11-0093

Bravo A, York T, Pumplin N, Mueller LA, Harrison MJ. Genes conserved for arbuscular mycorrhizal symbiosis identified through phylogenomics. *Nat Plants*. 2016:2(2):15208. https://doi.org/10.1038/nplants.2015.208

Brottier L, Chaintreuil C, Simion P, Scornavacca C, Rivallan R, Mournet P, Moulin L, Lewis GP, Fardoux J, Brown SC, et al. A phylogenetic framework of the legume genus *Aeschynomene* for comparative genetic analysis of the nod-dependent and nod-independent symbioses. *BMC Plant Biol*. 2018:18(1):333. https://doi.org/10.1186/s12870-018-1567-z

Buendia L, Girardin A, Wang T, Cottret L, Lefebvre B. Lysm receptor-like kinase and LysM receptor-like protein families: an update on phylogeny and functional characterization. *Front Plant Sci*. 2018:9:1531. https://doi.org/10.3389/fpls.2018.01531

Cabau C, Escudié F, Djari A, Guiguen Y, Bobe J, Klopp C. Compacting and correcting Trinity and oases RNA-Seq de novo assemblies. *PeerJ*. 2017:5:e2988. https://doi.org/10.7717/peerj.2988

Capella-Gutiérrez S, Silla-Martínez JM, Gabaldón T. Trimal: a tool for automated alignment trimming in large-scale phylogenetic analyses. *Bioinformatics*. 2009:25(15):1972–1973. https://doi.org/10.1093/bioinformatics/btp348

Cassan O, Lèbre S, Martin A. Inferring and analyzing gene regulatory networks from multi-factorial expression data: a complete and interactive suite. *BMC Genomics*. 2021:22(1):387. https://doi.org/10.1186/s12864-021-07659-2

Chaintreuil C, Perrier X, Martin G, Fardoux J, Lewis GP, Brottier L, Rivallan R, Gomez-Pacheco M, Bourges M, Lamy L, et al. Naturally occurring variations in the nod-independent model legume *Aeschynomene evenia* and relatives: a resource for nodulation genetics. *BMC Plant Biol*. 2018:18(1):54. https://doi.org/10.1186/s12870-018-1260-2

Chaintreuil C, Rivallan R, Bertioli DJ, Klopp C, Gouzy J, Courtois B, Leleux P, Martin G, Rami JF, Gully D, et al. A gene-based map of the nod factor-independent *Aeschynomene evenia* sheds new light on the evolution of nodulation and legume genomes. *DNA Res*. 2016:23(4):365–376. https://doi.org/10.1093/dnares/dsw020

Couzigou JM, Zhukov V, Mondy S, Abu el Heba G, Cosson V, Ellis TH, Ambrose M, Wen J, Tadege M, Tikhonovich I, et al. *NODULE ROOT* and *COCHLEATA* maintain nodule development and are legume orthologs of *Arabidopsis BLADE-ON-PETIOLE* genes. *Plant Cell*. 2012:24(11):4498–4510. https://doi.org/10.1105/tpc.112.103747

Ding Y, Lesterps Z, Gasciolli V, Fuchs AL, Gaston M, Medioni L, de-Regibus A, Remblière C, Vicédo C, Bensmihen S, et al. 2025. Several groups of LysM-RLKs are involved in symbiotic signal perception and arbuscular mycorrhiza establishment. Nat Commun. 2025:16:5999. https://doi.org/10.1038/s41467-025-60717-1

Ding Y, Wang T, Gasciolli V, Reyt G, Remblière C, Marcel F, François T, Bendahmane A, He G, Bono JJ, et al. The LysM receptor-like kinase SlLYK10 controls lipochitooligosaccharide signaling in inner cell layers of tomato roots. *Plant Cell Physiol*. 2024:65(7):1149–1159. https://doi.org/10.1093/pcp/pcae035

Dorjgotov D, Jurca ME, Fodor-Dunai C, Szucs A, Otvös K, Klement E, Bíró J, Fehér A. Plant rho-type (rop) GTPase-dependent activation of receptor-like cytoplasmic kinases *in vitro*. *FEBS Lett*. 2009:583(7):1175–1182. https://doi.org/10.1016/j.febslet.2009.02.047

Dunn OJ. Multiple comparisons using rank sums. *Technometrics*. 1964:6(3):241–252. https://doi.org/10.1080/00401706.1964.10490181

Fabre S, Gully D, Poitout A, Patrel D, Arrighi JF, Giraud E, Czernic P, Cartieaux F. Nod factor-independent nodulation in *Aeschynomene evenia* required the common plant-microbe symbiotic toolkit. *Plant Physiol*. 2015:169(4):2654–2664. https://doi.org/10.1104/pp.15.01134

Feng F, Sun J, Radhakrishnan GV, Lee T, Bozsóki Z, Fort S, Gavrin A, Gysel K, Thygesen MB, Andersen KR, et al. A combination of chitooligosaccharide and lipochitooligosaccharide recognition promotes arbuscular mycorrhizal associations in *Medicago truncatula*. *Nat Commun*. 2019:10(1):5047. https://doi.org/10.1038/s41467-019-12999-5

Fliegmann J, Jauneau A, Pichereaux C, Rosenberg C, Gasciolli V, Timmers AC, Burlet-Schiltz O, Cullimore J, Bono JJ. LYR3, a high-affinity LCO-binding protein of *Medicago truncatula*, interacts with LYK3, a key symbiotic receptor. *FEBS Lett*. 2016:590(10):1477–1487. https://doi.org/10.1002/1873-3468.12191

Girardin A, Wang T, Ding Y, Keller J, Buendia L, Gaston M, Ribeyre C, Gasciolli V, Auriac MC, Vernié T, et al. LCO receptors involved in arbuscular mycorrhiza are functional for rhizobia perception in legumes. *Curr Biol*. 2019:29(24):4249–4259.e5. https://doi.org/10.1016/j.cub.2019.11.038

Giraud E, Moulin L, Vallenet D, Barbe V, Cytryn E, Avarre JC, JaubertM, Simon D, Cartieaux F, Prin Y, et al. Legumes symbioses: absence of nod genes in photosynthetic bradyrhizobia. *Science*. 2007:316(5829):1307–1312. https://doi.org/10.1126/science.1139548

Gobbato E. Recent developments in arbuscular mycorrhizal signaling. *Curr Opin Plant Biol*. 2015:26:1–7. https://doi.org/10.1016/j.pbi.2015.05.006

Gully D, Czernic P, Cruveiller S, Mahé F, Longin C, Vallenet D, François P, Nidelet S, Rialle S, Giraud E, et al. Transcriptome profiles of nod factor-independent symbiosis in the tropical legume *Aeschynomene evenia*. *Sci Rep*. 2018:8:10934. https://doi.org/10.1038/s41598-018-29301-0

Hoang D, Chernomor O, von Haeseler A, Minh BQ, Vinh LS. UFBoot2: improving the ultrafast bootstrap approximation. *Mol Biol Evol*. 2018:35(2):518–522. https://doi.org/10.1093/molbev/msx281

Horta Araújo N, Nouwen N, Arrighi JF. Nodulating another way: what can we learn from lateral root base nodulation in legumes? *J Exp Bot*. 2024:75(11):3214–3219. https://doi.org/10.1093/jxb/erae101

Irving TB, Chakraborty S, Ivanov S, Schultze M, Mysore KS, Harrison MJ, Ané JM. KIN3 impacts arbuscular mycorrhizal symbiosis and promotes fungal colonisation in *Medicago truncatula*. *Plant J*. 2022:110(2):513–528. https://doi.org/10.1111/tpj.15685

Kalyaanamoorthy S, Minh BQ, Wong TKF, von Haeseler A, Jermiin LS. ModelFinder: fast model selection for accurate phylogenetic estimates. *Nat Methods*. 2017:14(6):587–589. https://doi.org/10.1038/nmeth.4285

Katoh K, Rozewicki J, Yamada K. MAFFT online service: multiple sequence alignment, interactive sequence choice and visualization. *Brief Bioinform*. 2019:20(4):1160–1166. https://doi.org/10.1093/bib/bbx108

Kawaharada Y, Kelly S, Nielsen MW, Hjuler CT, Gysel K, Muszyński A, Carlson RW, Thygesen MB, Sandal N, Asmussen MH, et al. Receptor-mediated exopolysaccharide perception controls bacterial infection. *Nature*. 2015:523(7560):308–312. https://doi.org/10.1038/nature14611

Klaus-Heisen D, Nurisso A, Pietraszewska-Bogiel A, Mbengue M, Camut S, Timmers T, Pichereaux C, Rossignol M, Gadella TW, Imberty A, et al. Structure-function similarities between a plant receptor-like kinase and the human interleukin-1 receptor-associated kinase-4. *J Biol Chem*. 2011:286(13):11202–11210. https://doi.org/10.1074/jbc.M110.186171

Kruskal WH, Wallis WA. Use of ranks in one-criterion variance analysis. *J Am Stat Assoc*. 1952:47(260):583–621. https://doi.org/10.1080/01621459.1952.10483441

Landry D, Mila I, Sabbagh CRR, Zaffuto M, Pouzet C, Tremousaygue D, Dabos P, Deslandes L, Peeters N. An NLR integrated domain toolkit to identify plant pathogen effector targets. *Plant J*. 2023:115(5):1443–1457. https://doi.org/10.1111/tpj.16331

Lee DS, Kim YC, Kwon SJ, Ryu CM, Park OK. The Arabidopsis cysteine-rich receptor-like kinase CRK36 regulates immunity through interaction with the cytoplasmic kinase BIK1. *Front Plant Sci*. 2017:8:1856. https://doi.org/10.3389/fpls.2017.01856

Lefebvre B, Klaus-Heisen D, Pietraszewska-Bogiel A, Hervé C, Camut S, Auriac MC, Gasciolli V, Nurisso A, Gadella TW, Cullimore J. Role of N-glycosylation sites and CXC motifs in trafficking of *Medicago truncatula* nod factor perception protein to plasma membrane. *J Biol Chem*. 2012:87(14):10812–10823. https://doi.org/10.1074/jbc.M111.281634

Leng J, Wei X, Jin X, Wang L, Fan K, Zou K, Zheng Z, Saridis G, Zhao N, Zhou D, et al. ARBUSCULAR MYCORRHIZA-INDUCED KINASES AMK8 and AMK24 associate with the receptor-like kinase KINASE3 to regulate arbuscular mycorrhizal symbiosis in *Lotus japonicus*. *Plant Cell*. 2023:35(6):2006–2026. https://doi.org/10.1093/plcell/koad050

Letunic I, Bork P. Interactive tree of life (iTOL) v6: recent updates to the phylogenetic tree display and annotation tool. *Nucleic Acids Res*. 2024:52(W1):W78–W82. https://doi.org/10.1093/nar/gkae268

Liang X, Zhou JM. Receptor-like cytoplasmic kinases: central players in plant receptor kinase-mediated signaling. *Annu Rev Plant Biol*. 2018:69(1):267–299. https://doi.org/10.1146/annurev-arplant-042817-040540

Lin W, Ma X, Shan L, He P. Big roles of small kinases: the complex functions of receptor-like cytoplasmic kinases in plant immunity and development. *J Integr Plant Biol*. 2013:55(12):1188–1197. https://doi.org/10.1111/jipb.12071

Minh BQ, Schmidt HA, Chernomor O, Schrempf D, Woodhams MD, von Haeseler A, Lanfear R. IQ-TREE 2: new models and efficient methods for phylogenetic inference in the genomic era. *Mol Biol Evol*. 2020:37(5):1530–1534. https://doi.org/10.1093/molbev/msaa015

Molendijk AJ, Ruperti B, Singh MK, Dovzhenko A, Ditengou FA, Milia M, Westphal L, Rosahl S, Soellick TR, Uhrig J, et al. A cysteine-rich receptor-like kinase NCRK and a pathogen-induced protein kinase RBK1 are rop GTPase interactors. *Plant J*. 2008:53(6):909–923. https://doi.org/10.1111/j.1365-313X.2007.03384.x

Montero H, Lee T, Pucker B, Ferreras-Garrucho G, Oldroyd G, Brockington SF, Miyao A, Paszkowski U. A mycorrhiza-associated receptor-like kinase with an ancient origin in the green lineage. *Proc Natl Acad Sci U S A*. 2021:118(25):e2105281118. https://doi.org/10.1073/pnas.2105281118

Nouwen N, Pervent M, El M'Chirgui F, Tellier F, Rios M, Horta Araújo N, Klopp C, Gressent F, Arrighi JF. OROSOMUCOID PROTEIN 1 regulation of sphingolipid synthesis is required for nodulation in *Aeschynomene evenia*. *Plant Physiol*. 2024:194(3):1611–1630. https://doi.org/10.1093/plphys/kiad642

Patel H, Ewels P, Manning J, Garcia MU, Peltzer A, Hammarén R, Botvinnik O, Talbot A, Sturm G, nf-core bot, et al. nf-core/rnaseq: nf-core/rnaseq v3.14.0 - hassium honey badger (3.14.0). *Zenodo* 2024:10471647.

Quilbé J, Lamy L, Brottier L, Leleux P, Fardoux J, Rivallan R, Benichou T, Guyonnet R, Becana M, Villar I, et al. Genetics of nodulation in *Aeschynomene evenia* uncovers mechanisms of the rhizobium-legume symbiosis. *Nat Commun*. 2021:12(1):829. https://doi.org/10.1038/s41467-021-21094-7

Quilbé J, Nouwen N, Pervent M, Guyonnet R, Cullimore J, Gressent F, Araújo NH, Gully D, Klopp C, Giraud E, et al. A mutant-based analysis of the establishment of nod-independent symbiosis in the legume *Aeschynomene evenia*. *Plant Physiol*. 2022:190(2):1400–1417. https://doi.org/10.1093/plphys/kiac325

Radhakrishnan GV, Keller J, Rich MK, Vernié T, Mbadinga Mbadinga DL, Vigneron N, Cottret L, Clemente HS, Libourel C, Cheema J, et al. An ancestral signalling pathway is conserved in intracellular symbioses-forming plant lineages. *Nat Plants*. 2020:6(3):280–289. https://doi.org/10.1038/s41477-020-0613-7

R Core Team. *R: a language and environment for statistical computing*. R Foundation for Statistical Computing; 2020. www.R-project.org/.

Rich MK, Vigneron N, Libourel C, Keller J, Xue L, Hajheidari M, Radhakrishnan GV, Le Ru A, Diop SI, Potente G, et al. Lipid exchanges drove the evolution of mutualism during plant terrestrialization. *Science*. 2021:372(6544):864–868. https://doi.org/10.1126/science.abg0929

Roth R, Chiapello M, Montero H, Gehrig P, Grossmann J, O'holleran K, Hartken D, Walters F, Yang SY, Hillmer S, et al. A rice Serine/Threonine receptor-like kinase regulates arbuscular mycorrhizal symbiosis at the peri-arbuscular membrane. *Nat Commun*. 2018:2:4677. https://doi.org/10.1038/s41467-018-06865-z

Roy S, Liu W, Nandety RS, Crook A, Mysore KS, Pislariu CI, Frugoli J, Dickstein R, Udvardi MK. Celebrating 20 years of genetic discoveries in legume nodulation and symbiotic nitrogen fixation. *Plant Cell*. 2020:32(1):15–41. https://doi.org/10.1105/tpc.19.00279

van Velzen R, Doyle JJ, Geurts R. A resurrected scenario: single gain and massive loss of nitrogen-fixing nodulation. *Trends Plant Sci*. 2019:24(1):49–57. https://doi.org/10.1016/j.tplants.2018.10.005

Vij S, Giri J, Dansana PK, Kapoor S, Tyagi AK. The receptor-like cytoplasmic kinase (OsRLCK) gene family in rice: organization, phylogenetic relationship, and expression during development and stress. *Mol Plant*. 2008:1(5):732–750. https://doi.org/10.1093/mp/ssn047

Voinnet O, Rivas S, Mestre P, Baulcombe D. An enhanced transient expression system in plants based on suppression of gene silencing by the p19 protein of tomato bushy stunt virus. *Plant J*. 2003:33(5):949–956. https://doi.org/10.1046/j.1365-313X.2003.01676.x

Wickham H. *Ggplot2: elegant graphics for data analysis*. New York: Springer-Verlag; 2016.

Zhang J, Sun J, Chiu CH, Landry D, Li K, Wen J, Mysore KS, Fort S, Lefebvre B, Oldroyd GED, et al. A receptor required for chitin perception facilitates arbuscular mycorrhizal associations and distinguishes root symbiosis from immunity. *Curr Biol*. 2024:34(8):1705–1717. https://doi.org/10.1016/j.cub.2024.03.015